HELSINGIN YLIOPISTO
HELSINGFORS UNIVERSITET
UNIVERSITY OF HELSINKI

MATEMAATTIS-LUONNONTIETEELLINEN TIEDEKUNTA
MATEMATISK-NATURVETENSKAPLIGA FAKULTETEN
FACULTY OF SCIENCE

Tiedekunta – Fakultet – Faculty Faculty of Science		Koulutusohjelma – Utbildningsprogram – Degree programme Theoretical physics
Tekijä – Författare – Author Ilkka Paalanen		
Työn nimi – Arbetets titel – Title Perturbative QCD at high density		
Työn laji – Arbetets art – Level Master's thesis	Aika – Datum – Month and year 4/2020	Sivumäärä – Sidoantal – Number of pages 62

Tiivistelmä – Referat – Abstract

Cold quark matter is matter consisting of free quarks in high energy density, and it can be formed when the energy density of ordinary hadronic matter increases to a region of 1 GeV/fm^3. At such high energies, hadronic matter undergoes a phase transition and quarks that would normally be in color confinement break free to form a new phase. It is assumed that similar process happened in the very early universe, but in the opposite direction, when high temperature quark-gluon plasma cooled down significantly. With the cooling, the quark and gluon degrees of freedom switched to hadrons and ordinary matter began to form. Opposed to the hot quark-gluon plasma, there are no direct observations of cold quark matter and its existence is still speculative. Still, it is suspected that cold quark matter can be found in dense neutron star cores or even as stable quark matter in strange quark stars.

Theoretically, cold quark matter and quark-gluon plasma can be studied in finite-temperature field theory. Finite-temperature field theory combines the field formalism of quantum field theory and the thermodynamical and statistical methods utilized in quantum statistics. The asymptotic freedom of the theory of strong interactions, quantum chromodynamics (QCD), provides an opportunity to expand the equation of state of high-energy quark matter in the limit of weak coupling, and thus opens a door to implement the tools of finite-temperature field theory perturbatively.

Along with the perturbative analysis, it is useful to look at the possibilities offered by effective theories. Two of which are important in the study of finite-temperature QCD, dimensional reduction and hard thermal loop effective theory. Both effective theories address the issue of infrared divergences that arise in finite-temperature field theory efficiently compared to the naïve loop expansion.

In dimensional reduction, scales that are defined as hard by the scale hierarchy are integrated out of the theory, after which the infrared problems of gluonic Matsubara zero-modes can be studied in a simpler three-dimensional setting. Hard thermal loop effective theory, on the other hand, examines the infrared divergences that appear in loop-level corrections of soft gluons. When the magnitude of the loop-momentum corresponds to the hard scale, the correction that contains the loop becomes proportional to a tree-level amplitude and breaks the perturbative expansion. The effective theory answers this problem by resumming the propagators and vertex functions and using the new quantities in place of the ordinary ones.

With perturbation theory and the effective descriptions, the equation of state of cold quark matter and the pressure extracted from it, have been solved partially up to and including order $g^6 \ln^2 g^2$ in coupling. The meaning of this thesis is to present the methods of finite-temperature field theory and the supporting effective theories and their implementation to study the equation of state of cold quark matter. The results for QCD pressure will be presented to the last known order in coupling. Also, the effect of a massive strange quark and the role of cold quark matter in solving the neutron star equation of state will be discussed briefly.

Avainsanat – Nyckelord – Keywords
Thermal field theory, QCD, perturbation theory, strong interaction, quark matter, neutron star, hard thermal loops

Säilytyspaikka – Förvaringställe – Where deposited

Muita tietoja – Övriga uppgifter – Additional information

Master's thesis

Theoretical physics

Perturbative QCD at high density

Ilkka Paalanen

2020

Supervisor: Aleksi Vuorinen

Examiners: Aleksi Vuorinen

Kimmo Tuominen

University of Helsinki

Department of Physics

PL 64 (Gustaf Hällströmin katu 2)

00014 Helsingin yliopisto

Contents

1 Introduction: QCD at high density

The emergence of quantum chromodynamics (QCD) followed the success of the field theoretic description of particle physics that was breaking ground in the mid 20th century. The accuracy of predictions made in quantum electrodynamics led others to try the same approach with strong interactions. Through the invention of the quark model and the probing of nuclei in deep inelastic scattering experiments in the 60s and early 70s, a gauge theory of strongly interacting quarks and gluons stabilized its position as a fundamental theory of Nature [1]. Up to this day, the QCD framework has been applied to numerous situations from scattering experiments to studying the origins of the Universe.

The aim of this thesis is to study the effects of strong interactions on the relations of thermodynamic variables, described as the equation of state (EoS), of quark matter in a setting of high density and low temperature. Such a scenario could correspond to e.g. a compact neutron star with a quark core or a star composed purely of stable quark matter [2].

1.1 Characteristics of QCD

QCD is a non-Abelian gauge theory with a corresponding symmetry group SU(3), the group generators of which are related to the eight massless gluon fields. The gauge symmetry is often labelled as color symmetry which underlines the nature of strong interactions, as the conserved quantity, analogous to electric charge in QED, is defined as "color". However, the dynamics of

QCD interactions is slightly more intricate since the color charges come in a variety of three.

QCD is a non-Abelian gauge theory and it is asymptotically free, which means that the QCD beta function is negative: the coupling decreases at high energy scale [3]. Along with the confinement of quarks, the asymptotic freedom is one of the two defining characteristics of strong interactions. At relatively long distances (low energy scale) the QCD coupling grows too large to be treated perturbatively and quarks are strongly confined to form hadrons, and cannot be isolated as free particles. Vice versa, at short distances (high energy scale) the coupling goes effectively to zero leaving quarks to behave as free "point particles" void of interactions.

In its simplest form the Lagrangian describing QCD interactions can be written as [4]

$$\mathcal{L}_{QCD} = -\frac{1}{4}F^a_{\mu\nu}F_a^{\mu\nu} + \bar{\psi}(i\not{D}_\mu - m)\psi, \tag{1.1}$$

where ψ is a color triplet under SU(3), $D_\mu = i\partial_\mu - gA^a_\mu G_a$ is the covariant derivative in the fundamental representation, A^a_μ are the gauge fields, and the mass matrix m is diagonal in flavour space. The gluon field strength tensor is defined as

$$F^a_{\mu\nu} = \partial_\mu A^a_\nu - \partial_\nu A^a_\mu - g f_{abc} A^b_\mu A^c_\nu. \tag{1.2}$$

The SU(3) generators $G^a = \frac{\lambda^a}{2}$ and the structure constants f^{abc} satisfy commutation relations $[\frac{\lambda^a}{2}, \frac{\lambda^b}{2}] = if^{abc}\frac{\lambda^c}{2}$, and trace identities of the generators read as $\mathrm{Tr}[\frac{\lambda^a}{2}\frac{\lambda^b}{2}] = \frac{\delta^{ab}}{2}$. The λ^a are the famous Gell-Mann matrices, with $a = 1, \ldots, N^2 - 1$ (for SU(3) the number of generators is naturally eight).

The Lagrangian is invariant under the transformations [5]

$$A^a_\mu \to A^a_\mu + \partial_\mu\theta^a + g f_{abc} A^b_\mu \theta^c + \mathcal{O}(\theta^2), \tag{1.3}$$

$$\psi \to \psi + ig\theta^a G_a \psi + \mathcal{O}(\theta^2). \tag{1.4}$$

The transformations are generated by a local operator $U = exp(ig\theta^a(x)G_a)$,

under which the gauge fields transform in the adjoint and the quark fields in the fundamental representation.

The above equations define the theory of QCD interactions completely [6], but as will be shown later, quantization of the theory will apply modifications, such as unphysical ghost particles and a gauge fixing term, to the Lagrangian, as well as introducing a chemical potential as a bridge from the vacuum to finite density QCD.

1.2 Finite density via chemical potential

In classical statistical mechanics, chemical potential is defined as a conjugate variable to the particle number N. It gives the change of free energy with respect to N, by the well known equation $dF = -VdP - SdT + \mu dN$, where V, P, S, T and μ are volume, pressure, entropy, temperature and chemical potential, respectively, and serves the purpose of a Lagrange multiplier in particle number conservation [7]. The (quantum) statistical properties of any thermodynamic system can be embedded in an object called a partition function which is defined as

$$\mathcal{Z}(T,\mu) = \mathrm{Tr}[e^{-\beta(\hat{H}-\mu\hat{N})}], \tag{1.5}$$

where the trace is taken over the Fock space, with $\hat{H}$ being the Hamiltonian and $\hat{N}$ the number operator.

When studying systems with finite density, one is interested in finite chemical potential. It is associated to particles with non-zero charge, but aside from its usefulness in calculations, physical properties are better understood by the conjugate variable, number density of the conserved charge [5]. Hence, the connection between chemical potential and finite density becomes apparent.

When studying QCD at finite density, chemical potential connects to the Lagrangian by the conserved Noether current of a global symmetry where

$\psi \to e^{-i\alpha}\psi$,

$$\mathcal{J}_\mu = \bar{\psi}\gamma_\mu\psi. \tag{1.6}$$

The vector current then gives rise to an effective Hamiltonian, similar to the partition function of equation (1.5), $\hat{H} - \mu\hat{Q}$, where the charge is the usual zero component of the current density

$$Q = \int_{\mathbf{x}} \bar{\psi}\gamma_0\psi. \tag{1.7}$$

Thus the Lagrangian gets a following contribution [5]

$$\mathcal{L}_{QCD} + \Delta\mathcal{L} = -\frac{1}{4}F^a_{\mu\nu}F_a^{\mu\nu} + \bar{\psi}(\not{D}_\mu - m - \mu\gamma_0)\psi. \tag{1.8}$$

Flavour being a conserved global symmetry of QCD, the quark chemical potential separates into a sum of potentials of different quark flavours. The system in question sets constraints to the way chemical potentials are accounted for, e.g. in the limit of massless quarks one can consider a situation of equal chemical potentials for different flavours [8].

1.3 Deconfinement of quarks

The asymptotic freedom of QCD sets the stage for interesting phenomena occurring at high energy scales. At an energy density of around 1 GeV/fm^3, ordinary hadronic matter undergoes what is referred to as a deconfinement phase transition [4], during which the hadronic degrees of freedom break into the degrees of freedom of quarks and gluons [9]. This can happen when either the density or the temperature of the system increases vastly and goes past a critical point. The former case corresponds (at zero temperature) to a setting of cold quark matter which will be discussed more in the next section, and the latter to a system known as quark-gluon plasma (QGP).

The phase structure of the QGP has been under scrutiny for over two decades and understanding the elusive nature of deconfinement has been a rather tedious task [10]. Nevertheless, many successful studies in different

ranges of temperature and chemical potential have been made over the years. The initial point of the different approaches and approximations has been the same: solving and matching the equations of state of different phases. For deconfinement, phase transition means that the baryon number density must have a discontinuity at some critical chemical potential (cold quark matter) or temperature (QGP), which is used as a matching point for the hadronic and deconfined phase EoSs. The matching procedure is then constrained by various physical requirements, one of which being that the pressures of the two phases must meet at the matching point [2]. While sizable non-zero chemical potentials prevent the use of Monte Carlo simulations of the EoS, lattice QCD models have been able to shed light to physics around the critical deconfinement temperature at $\mu = 0$ [11]. Also, the asymptotic freedom of QCD at energy densities way over the deconfinement line of the phase diagram allows the use of perturbation theory in regimes of arbitrary μ and T, due to the smallness of the QCD coupling constant. Perturbative approaches have yielded results for the pressure of the QGP to high orders in coupling constant for different values of the ratio μ/T, and for high density and low temperature limit converges relatively well with the previous results of $T = 0$ [10].

Aside from the inherent theoretical interest of the subject, the deconfined phase plays a central role in some applications. One of these is related to the early stages of the Universe in a time scale of a few microseconds. As is understood by the standard big bang theory, primordial QGP underwent a crossover phase transition from the deconfined to the confined hadron phase [12]. In a crossover transition, thermodynamic variables and their derivatives transition smoothly (no discontinuities) from the deconfined to the confined phase. It was suggested that there could be a first order transition that would lead to baryon inhomogeneity which in turn would affect nucleosynthesis [13]. However, the nature of the crossover transition does

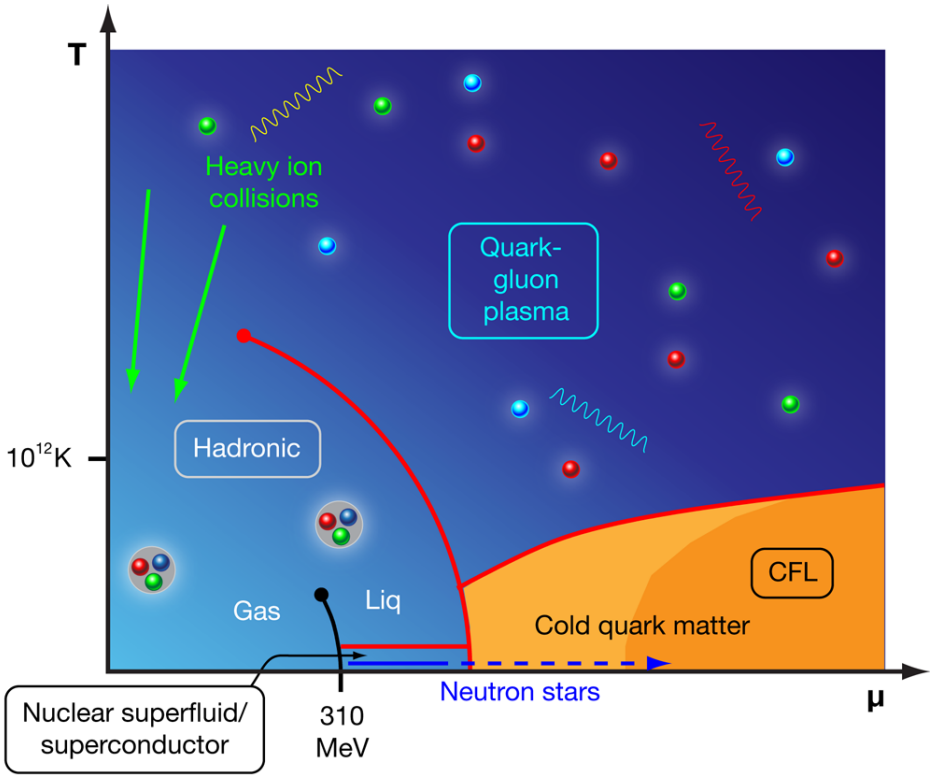

Figure 1.1: The phase diagram of QCD with respect to temperature and quark chemical potential. The CFL area describes a color-flavour-locked phase at extremely high densities, where the quark color and flavour properties are in direct correspondence. [14]

not accommodate such a mechanism and therefore cannot be a source of said inhomogeneity. Still, the QCD phase transition remains an important feature in the evolution of the Universe. A more relevant application in the framework of this thesis, relates to high density and cold quark matter.

1.4 Cold quark matter

At low temperatures the deconfinement of hadronic matter requires a high baryon chemical potential in order to occur. At such a high densities strange quarks may be produced through simultaneous weak interactions between

the hadron constituents and in right conditions achieve chemical equilibrium leading to a constraint to the quark chemical potentials [4]

$$\mu_s = \mu_d = \mu_u + \mu_e, \tag{1.9}$$

where the subscripts refer to the corresponding quark and electron. The existence of stable quark matter would render nucleons metastable (with a lifetime of billions of years) and form a ground state for nuclear matter. The equation of state for (strange) quark matter has been studied in thermal perturbation theory in a setting of high density and zero temperature, obtaining convergent results but little certainty of stability. While the theoretical results for a strange ground state remain inconclusive [2], the possibility of quark matter inside compact stellar cores is an intriguing prospect, as it does not require quark matter in vacuum to be absolutely stable.

Even though perturbative QCD is only applicable in the region of very high energy density, it is still useful in determining the properties of compact and dense neutron stars. The densities realized in the cores of neutron stars fall in a range between perturbation theory and nuclear-theory computations, and can be estimated by an ensemble of thermodynamically consistent polytropic EoSs suitable in this region. Recent gravitational wave data from a neutron star merger have given sound constraints to the neutron star EoS and boosted the precision of the EoS ensemble approach [15]. Figure 3.6 in chapter 3 illustrates well the matching of pressure as a function of energy density, obtained from nuclear-theory and pQCD, to the EoS ensemble.

As previously stated, the scope of this thesis is to study the perturbative expansion of the equation of state of quark matter (low T and high μ), namely the grand potential $\Omega = -T\ln\mathcal{Z} = -PV$. First, the needed machinery from thermal perturbation theory is introduced to evaluate the partition function in the weak coupling limit, by the courtesy of asymptotic freedom. Then, a closer look is given to the state-of-the-art pressure of quark matter,

collecting some of the latest results of the topic, after which first lowest order non-analytic contributions to the pressure are calculated, originating from the diagram corresponding to the so called hard-thermal-loop (HTL) ring sum.

2 Basics of perturbative thermal field theory

In this chapter main elements of extending perturbation theory to a system in thermal equilibrium are introduced. The effects of finite temperature and chemical potential bring adjustments to perturbative QCD and the observables one is interested in are extracted from the functional integral emerging from the path integral quantization of the quantum statistical partition function. The bulk thermodynamic properties of the thermal medium are best described in Euclidean space which is introduced from imaginary-time (IT) formulation of the theory. The general definitions in this chapter can be found from textbooks, mainly [4] and [5], focusing on the IT formalism of thermal perturbation theory.

2.1 Path integral of the partition function

Thermal and finite density effects can be described in a field theoretic setting by applying the well known relations of quantum statistical mechanics. For relativistic systems, such as the ones considered in this thesis, the natural thermodynamic framework is the grand canonical ensemble where the presence of particle number fluctuations is taken into account. To study the pressure of quark matter, one statistical equation becomes most important: the grand potential $-\Omega/V = P$ and its relation to the partition function. The

usual constraints of grand canonical ensemble apply also in field theory:

$$\langle \mathbf{1} \rangle = 1 \tag{2.1}$$

$$\langle \hat{H} \rangle = E \tag{2.2}$$

$$\langle \hat{N} \rangle = N. \tag{2.3}$$

Grand potential is linked to the grand canonical partition function by $\Omega = -T\ln\mathcal{Z}$. The partition function is a most important quantity as it contains all the information of the theory and system in question and thus can be used to obtain many interesting observables by known statistical relations.

Quantizing QCD for fermions and gauge fields with the partition function $\mathcal{Z} = \mathrm{Tr}[e^{-\beta(\hat{H}-\mu\hat{Q})}]$, where $\hat{Q}$ is the aforementioned conserved flavour charge operator, leads to a following path integral representation:

$$\begin{aligned}\mathcal{Z} = C \int_{\text{periodic}} \mathcal{D}A_0^a \mathcal{D}A_k^a \int_{\text{periodic}} \mathcal{D}\bar{c}^a \mathcal{D}c^a \int_{\text{anti-periodic}} \mathcal{D}\bar{\psi}_i \mathcal{D}\psi_i \times \\ \times \exp\Bigg(- \int_0^\beta \int_{\mathbf{x}} \frac{1}{4} F_{\mu\nu}^a F_{\mu\nu}^a + \frac{1}{2\rho} \partial_\mu A_\mu^a \partial_\nu A_\nu^a + \partial_\mu \bar{c}^a \partial_\mu c^a + \\ + g f^{abc} \partial_\mu \bar{c}^a A_\mu^b c^c + \bar{\psi}_i (\gamma_\mu D_\mu + m_i - \gamma_0 \mu_i) \psi_i \Bigg),\end{aligned} \tag{2.4}$$

where covariant gauges for the ghost field and gauge-fixing terms are applied. The derivation of this form is not of any particular interest in this thesis, but a few remarks should be made. An interesting note is that the path integral form resembles very much the time-evolution operator in vacuum QFT which is defined in a path integral representation as $[\exp(-i\hat{H}\Delta t)]_{lk} = \int_{\phi(t_0)=\phi_l}^{\phi(t_1)=\phi_k} \mathcal{D}\phi \, \exp[iS(\phi)]$, with the distinction that in the partition function Δt is replaced by the imaginary quantity $-i\beta$ for the Hamiltonian. The integration measures originate from removing discretization of the original trace in the partition function by splitting the operators to N infinitesimal pieces and after some algebra taking a limit $N \to \infty$. The integration regions, "periodic" and "anti-periodic", also originate from the traces and reflect bosonic and fermionic statistics, i.e. bosonic fields are equal at lower and

upper bound 0 and β while fermionic fields evaluate to $\psi(\beta) = -\psi(0)$ (same for $\bar{\psi}$). The ghost fields $\bar{c}^a$ and c^a, although being Grassmann in nature, must be periodic since they are needed to remove unphysical bosonic degrees of freedom from physical quantities. The appearance of the gauge-fixing term (with ρ the gauge parameter) is required for making a non-singular matrix to define gluon propagators. The subscript i in the quark fields imply summing over all quark flavours. The C in front of the integrals is a constant which vanishes in most cases and can be ignored.

As can be seen, the exponent of equation (2.9) contains the QCD action, but it is Euclidean in nature (implied also by keeping all the Lorentz indices lowered). The origins of this dramatic change of metric lie in the quantization of the theory in thermal equilibrium: the density operator defining the equilibrium is invariant under time translations which ensures the freedom to define the initial time in the functional integrals over the fields. Fields that are locally dependent on time disappear when initial and final time arguments are set equal leaving only the Euclidean part, hence the use of the Euclidean Lagrangian. Also, the integration limit β appears due to the quantization process. The original partition function couples the Hamiltonian and β as $\sim e^{-\beta\mathcal{H}}$ and as the discretization is removed (in quantization) by introducing continuous functions of the parameter τ, the (anti-)periodicity mentioned above requires the upper boundary to be equal to β.

To extract observables form the partition function it is convenient to split the action in it into free and interaction parts $\mathcal{Z} = \int \ldots e^{-S_0 - S_\mathrm{I}}$. Separating the free part and the interaction part to expand the exponential results in the following form for the grand potential:

$$\Omega/V = -T/V \ln\left[\mathcal{Z}_0 \left\langle 1 - \sum_{n>0} \frac{1}{n!} S_\mathrm{I}^n \right\rangle\right] \tag{2.5}$$

and the logarithm can be further expanded to give a useful expression:

$$\Omega/V = \Omega_0/V - T/V \left\langle \sum_{n>0} \frac{1}{n!} S_{\mathrm{I}}^n \right\rangle_{0,\mathrm{connected}} . \tag{2.6}$$

The expectation value is taken with respect to the free partition function (hence the subscript 0) and the label "connected" means that only fully connected diagrams are taken into account. This ensures that when using Wick's theorem to organize expectation values to combinations of two point correlation functions the disconnected parts cancel and evaluation of quantities such as the grand potential give meaningful results. The expectation values that arise from the evaluation of grand potential can be calculated with Feynman rules for thermal QCD in a similar way as in vacuum field theory.

2.2 Imaginary-time formalism

The Euclidean nature following from the path integral quantization induces a convenient way to handle bulk thermodynamics known as imaginary-time formalism. The fields, whose time dependence is now shifted to be purely imaginary ($\tau = -it$), are discretized in Fourier representation, while enforcing the earlier periodicity conditions, known as a Matsubara sum, which is convenient to do first with scalar fields (and staying at zero density) for clarity, by

$$\phi(\tau, \mathbf{x}) = T \sum_n \phi(\omega_n, \mathbf{x}) e^{i\omega_n \tau}.$$

Here, the sum over ω_n is taken over even or odd n depending on whether the field follows bosonic or fermionic statistics, with $\omega_n = 2\pi T n$ and $\omega_n = \pi T(2n+1)$ respectively, and the appearance of T in front of the sum is a convention. The spatial part of the above Matsubara sum of $\phi(\tau, \mathbf{x})$ can be taken to continuum in the usual way by imposing a limit of infinite volume. The same does not apply to the Matsubara modes unless the system is at zero

temperature, reducing the sum to an integral over the temporal component of the momentum. This implies the following form of bosonic and fermionic thermal sum-integrals:

$$\phi(\tau, \mathbf{x}) = \oint\!\!\!\!\!\!\sum_{P/\{P\}} \phi(\omega_n, \mathbf{p}) e^{-i(\omega_n \tau - \mathbf{p}\cdot\mathbf{x})}.$$

A few definitions appear to be in order. P is the Euclidean four-momentum (p_n, p_i), where p_n contains the Matsubara frequencies. Despite of Euclidean metric, the product of position ($X = (\tau, \mathbf{x})$) and momentum four-vectors appearing in propagators and correlation functions remains the same $X \cdot P = \tau p_n - \mathbf{x} \cdot \mathbf{p}$. The sum-integral combines the discrete Matsubara sum and the spatial continuum integral as

$$\oint\!\!\!\!\!\!\sum_{P/\{P\}} \equiv T \sum_n \int \frac{d^d p}{(2\pi)^d}. \tag{2.7}$$

Here the subscripts P and $\{P\}$ tell the nature of the summation, curly brackets implying that the sum is taken over anti-periodic frequencies; the sums are referred to as bosonic and fermionic thermal sums.

For a generic meromorphic function $f(p)$ the bosonic thermal sum can be evaluated as a complex integral with the help of the Bose distribution function. The distribution function (multiplied by i)

$$i n_b(ip) = \frac{i}{e^{ip\beta} - 1} \tag{2.8}$$

has poles at $p\beta = 2\pi n$ giving p precisely as the bosonic Matsubara frequencies $\omega_n = 2\pi n T$, with a degenerate residue of T at each pole. This allows the thermal sum for $f(p)$ to be converted to a contour integral

$$T \sum_{2n} f(\omega_n) = \oint f(p) i n_b(ip). \tag{2.9}$$

Fermionic thermal sums are connected to the bosonic ones by a simple rule

$$\sigma_f \equiv T \sum_{2n+1} f(\omega_n) = 2\sigma_b(T/2) - \sigma_b(T), \tag{2.10}$$

where σ_b represents the bosonic sum.

IT-formalism can be implemented to the Minkowski Lagrangian directly reflecting the quantization process. When the temporal field components are shifted, a shift must also occur in the (covariant) derivatives $\partial_t \to i\partial_\tau$ ($D_t \to iD_\tau$) and the temporal gauge field $A_0^a \to iA_0^a$. Euclidean Lagrangian is defined then through $L_E = -\mathcal{L}_M(t = -i\tau)$. With these modifications the Euclidean QCD Lagrangian reads

$$L_E = \frac{1}{4}F^a_{\mu\nu}F^a_{\mu\nu} + \bar{\psi}(\not{D}_\mu + m - \gamma_0\mu), \tag{2.11}$$

where the use of Euclidean metric is again implied by keeping the Lorentz indices lowered when summed over. Obviously, the Euclidean Lagrangian implies Euclidean propagators as well.

Inverting the matrices in the free action of eq. (2.9) gives the following momentum-space free propagators for gluons, ghosts and fermions:

$$\langle \tilde{A}(P)^a_\mu \tilde{A}(Q)^b_\nu \rangle_0 = \delta^{ab}\delta(P+Q)\left[\frac{\delta_{\mu\nu} - \frac{P_\mu P_\nu}{P^2}}{P^2} + \frac{\frac{\rho P_\mu P_\nu}{P^2}}{P^2}\right] \tag{2.12}$$

$$\langle \tilde{c}(P)^a \tilde{\bar{c}}(Q)^b \rangle_0 = \delta^{ab}\delta(P-Q)\frac{1}{P^2} \tag{2.13}$$

$$\langle \tilde{\psi}(P)_A \tilde{\bar{\psi}}(Q)_B \rangle_0 = \delta_{AB}\delta(P-Q)\frac{-i\not{P} + m}{P^2 + m^2}. \tag{2.14}$$

The $\delta(P \pm Q)$ can be treated as an ordinary $d+1$ dimensional delta function when e.g. integrated over, and is defined as $\delta_{p_n \pm q_n, 0}\delta^{(d)}(\mathbf{p} \pm \mathbf{q})$. Also the gauge-fixing parameter (ρ) dependence of the gluon free propagator appears as expected. The capital letters A and B in the quark fields contain both color and flavour indices. The most important part of these equations manifests itself in the right hand side of eq. (2.14) when $\not{P}$ and P^2 are opened explicitly as

$$\frac{-i\not{P} + m}{P^2 + m^2} = \frac{-i(\gamma_0 p_n + \gamma_0 i\mu + \gamma_i p_i) + m}{(p_n + i\mu)^2 + p^2 + m^2}. \tag{2.15}$$

This is how finite density i.e. the chemical potential appears in observables through diagrams: it corresponds to a shift $p_n \to p_n + i\mu$ in Matsubara frequencies of fermionic lines in Feynman diagrams. Three- and four-gluon,

fermion interaction and ghost interaction vertex functions are defined from the interaction part S_I, but it is not necessary to write them out explicitly, since they offer little insight apart from computational details. Momentum space Feynman rules can be found from textbooks, e.g. [5].

Alas, the naive perturbative expansion of the grand potential in the imaginary-time set-up is not itself sufficient to provide the physical quantities one is usually after. As in vacuum QFT, loop diagrams diverge in the ultraviolet region ($P \to \infty$) and the divergence is of course transported to observables. To counter this undesirable effect also thermal field theories have to be renormalized. Another issue is that when taking the opposite limit ($P \to 0$), i.e. going to the infrared region, massless propagators diverge, which is the case for e.g. gluons. This is also seen in, for example, free energy when one uses only the naive expansion, but can be corrected with proper handling of the IR divergences, known as resummation.

2.3 Renormalization, thermal mass and resummation

Renormalization of QCD at finite densities and temperatures is not different from that of vacuum QCD. The unphysical ultraviolet divergences appearing in integrals at short distances disappear through zero-temperature renormalization [5] of the bare coupling and fermion mass parameters. Hence, the renormalized quark mass and coupling can be evaluated without any thermal

or finite density treatment up to g^4 as [16]

$$g_b^2 = g_r^2 Z_g = g_r^2\left[1 - \frac{\alpha_s}{4\pi}(\frac{11}{3}C_A - \frac{4}{3}\frac{N_f}{2})\frac{1}{\epsilon}\right] \tag{2.16}$$

$$m_b^2 = m_r^2 Z_m = m_r^2\Bigg[1 - \frac{\alpha_s}{4\pi}(3C_F)\frac{1}{\epsilon} + \\ + \left(\frac{\alpha_s}{4\pi}\right)^2 C_F\Big((\frac{11}{2}C_A - N_f + \frac{9}{2}C_F)\frac{1}{\epsilon^2} - (\frac{97}{12}C_A - \frac{5}{6}N_f + \frac{3}{4}C_F)\frac{1}{\epsilon}\Big)\Bigg], \tag{2.17}$$

with α_s the running strong coupling, N_f the flavour number and the group theoretic factors defined as $C_F = \frac{N_c^2-1}{2N_c}$ and $C_A = N_c$, N_c being the number of colors in SU(N_c). ϵ originates from dimensional regulation, where loop integrals that diverge at four dimensions are evaluated in $d = 4-\epsilon$ dimensions instead. The divergences are thus captured in the ϵ parameter.

Working in the infrared sector on the other hand is significantly different in a thermal and finite density environment. Gluons being massless suffer divergences in long wavelengths while fermions even in massless limit are safe in the infrared region. This comes from the effect of the Matsubara frequencies in the denominators of sum-integrals, when finite temperatures are considered. For fermions, there exists no zero mode, meaning that the denominators are always weighted by some order of $(\pi T)^2$ even in long wavelengths $k^2 \to 0$ making thermal corrections that appear at order $(gT)^2$ or $(g\mu)^2$ subleading in the weak coupling expansion. Gluons however must be corrected with something called thermal (or effective) mass since bosonic statistics have a $n = 0$ part in the thermal sums and the corrections thus give a significant contribution. Physically this means that propagation in a thermal medium comes at a cost of screening of the temporal gauge field; to leading order the thermal mass originates from the longitudinal part of the gluon polarization tensor, because transverse structure vanishes in the infrared region, giving [17]

$$m_{eff}^2 = \Pi_{00}(k_0 = 0, k = -m_{eff}^2) = g^2\left((\frac{N_c}{3} + \frac{N_f}{6})T^2 + \frac{1}{2\pi^2}\sum_f \mu_f^2\right). \tag{2.18}$$

Thermal mass for ghosts has no physical meaning as it rather corresponds to a wave function normalization than a "mass correction".

The divergences manifesting in the infrared limit of gluonic momenta pose a serious problem in the naive loop expansion of the equation of state. A remedy for this obstacle is a method called resummation. General idea behind it is to identify and sum over all divergent terms which then together construct IR convergent quantities. The zero modes get corrected by the thermal mass mentioned above yielding a finite result where the divergent terms cancel order by order. Calculating every order in the loop expansion becomes increasingly cumbersome as one proceeds to higher orders, so using the perturbative approach is somewhat limited. Other methods labelled as effective theories have been harnessed to treat the troublesome resummation of the infrared sector revealing ever higher contributions. Next, a closer look is given to two of such effective theories: dimensional reduction (DR) and hard-thermal-loop effective theory.

2.4 Dimensional reduction

To capture the infrared effects causing trouble in perturbative QCD, in the case of high temperatures, it is sufficient to reduce the theory into an effective description and analyse only the problematic static sector plagued with the infrared divergences, i.e. soft contributions related to the Matsubara zero modes $k_0 = 0$. This formalism is called dimensional reduction, originating from the fact that when the soft contributions are considered, they do not depend on the imaginary time argument τ, reducing the appearing integrals to $3-2\epsilon$ spatial dimensions (in dimensional regularization) [5]. At tree level, this suggests a decoupling of the temporal gauge field (treated now as a scalar field in adjoint representation) from the spatial gauge fields which appear now as a three dimensional Yang-Mills potential of the reduced theory [18]. This reduction produces an effective theory called Electrostatic QCD

(EQCD). The details of dimensional reduction are not described explicitly here, because they are not needed in the calculations presented later, but are useful to understand in relation to some of the results of quark matter pressure.

Every thermal system possesses something referred to as a scale hierarchy. As an example, the temporal gauge field obtains the effective mass term by propagating in the thermal medium, resulting in exponential (Debye) screening, and effectively does not appear at long distances. This screening which produces the scales in thermal QCD consisting of bosonic and fermionic fields can be found by studying the (corrected) poles in the propagators. For fermions, at one-loop level, as there is no need for a mass correction the leading contribution comes from the discrete sum and is πT, giving a scale referred to as a hard scale. For the static modes, the scale was given earlier in terms of the effective mass, which was of order $m_{eff} \sim gT$ which is known as the soft scale. The final scale would correspond to the screening of zero-mode spatial gauge fields yielding the supersoft scale of g^2T. Thus the hierarchy can be stated as $g^2T \ll gT \ll \pi T$. The supersoft scale does not appear at one-loop level and in the present case is not necessary anyway since only the EQCD sector is of interest here. If one wishes to reduce the theory even further to study the g^2T scale, it would correspond to a pure three dimensional Yang-Mills theory, Magnetostatic QCD (MQCD).

To summarise the procedure, which can be applied to reduce 4D-QCD to EQCD, more generally [19], [5]: first the "unnecessary" degrees of freedom corresponding to the hard scale are integrated out to form the effective theory respecting all relevant symmetries (e.g. gauge, 3-dimensional rotation and required discrete symmetries); then, Green's functions determined from the effective theory are matched (and subtracted from) to the ones calculated with the full theory to obtain effective coupling and mass parameters, with which the infrared infested parts should cancel; in the final step, having

to deal with an infinite number of operators of increasing dimension, the operators in the effective Lagrangian need to be truncated at the desired order, producing an error to be evaluated by comparing the effect of the first operator left out with the truncated theory. If after this operation the IR divergences disappear and the truncation error is small relative to the order of the observables in question, the effective theory can be deemed successful.

As the main interest in this thesis is to study the pressure of quark matter, it should be pointed out how it is defined in these effective theories. To produce the full QCD pressure it is split into three parts that correspond to the momentum scales defined above as [10]:

$$p_{\mathrm{QCD}} = p_{\mathrm{4d,naive}} + p_{\mathrm{EQCD}} + p_{\mathrm{MQCD}}. \tag{2.19}$$

The first term on the right hand side is the pressure obtained from unresummed naive loop expansion of the full four dimensional theory. Next in line is the full (also unresummed) EQCD effective theory result that is calculated in the weak-coupling expansion, while the last term gives contributions from the MQCD sector that appear only at higher orders and need to be calculated via lattice field simulations. Together the combined pressure yields an IR finite result.

As stated afore, this procedure requires high enough temperature to be applicable. Nevertheless it is also useful concerning low-temperature quark matter. The qluonic medium modifications appearing with the polarization tensor are proportional to the thermal mass (2.18), so if the temperature of quark matter satisfies $T \gg m_{eff}$ being still relatively low, using dimensional reduction is justified. This indeed is the case for phenomena emerging in neutron star mergers where low-temperature nuclear matter, usually described with zero-temperature approximations, heats up enough to be evaluated with an effective theory [20]. In such a case, choosing the right tools can save a lot of work. For example, the infrared sensitive soft sector can be split

in two: static and non-static. The static sector can be efficiently treated in EQCD and the non-static sector which would be MQCD, can actually be evaluated more easily in the HTL framework.

2.5 Hard-Thermal-Loop effective theory

Hard thermal loops describe an infrared phenomenon where higher order contributions in perturbative expansion actually give something proportional to tree level amplitude, e.g. a loop correction of order g^2 yielding a result of order 1. Physically they originate from emissions and absorptions of particles in the thermal medium appearing as fluctuations due to high temperatures. A method called HTL power counting gives a tool to conceptualise the issue. At one-loop level for the gluon two-point function a general diagram imports a factor of g^2 with external legs contributing an external momentum dependency of $1/P^2$. When integrating over the loop momenta, the HTL contribution is obtained from the region where the internal momenta are said to be hard i.e. of order T, then calculating the loop integral gives a factor proportional to T^2. Combining these together one acquires a factor of g^2T^2/P^2 times a tree level amplitude corresponding to the same process [21]. The problem presents itself in the infrared region: if the external momentum is soft (infrared sensitive), then P is of order gT and the expansion parameter increases to be of $\mathcal{O}(1)$ implying a breakdown of the perturbation series when a loop in fact yields a term proportional to a tree level amplitude.

To overcome the apparent infrared problem, the HTL effective theory needs resummation as well. To carry out the resummation, instead of bare propagators and vertices, effective ones are used in a similar manner as in regular perturbation theory. This concerns only situations where every external leg in a vertex carries soft momentum. For propagators this means that the effective propagator consists of the bare propagator plus all parts of

the self energy tensor that contain a hard therman loop. In the same way, the bare three- and four-gluon and quark-gluon vertices obtain HTL corrections from one-loop insertions of hard thermal loops. To carry out the effective contributions in a compact way, they can be gathered inside an effecive action from which the effective propagators and vertices can be determined like always. This is the HTL effective theory. One can go even further and reorganize the QCD Lagrangian to include a HTL improvement term and use it alongside the perturbative expansion to build HTL petrurbation theory (in Minkowski space time for the time being) as [22]

$$\mathcal{L} = \mathcal{L}_{QCD} + \mathcal{L}_{HTL} + \Delta\mathcal{L}_{HTL}, \tag{2.20}$$

with

$$\mathcal{L}_{HTL} = -\frac{3}{2}m^2(1-\delta)\mathrm{Tr}\left[G_{\mu\alpha}\left\langle \frac{y^\alpha y^\beta}{(y\cdot D)^2} \right\rangle_y G^\mu_\beta \right]. \tag{2.21}$$

Here, D is the usual covariant derivative, the mass parameter m is the thermal mass, δ plays the role of an expansion parameter taken to one (i.e. the free limit when the improvement term vanishes from the original Lagrangian) only after determining the observables, and $y = (1, \hat{\mathbf{y}})$ is a light-like vector with the angle brackets signalling an average over all directions of $\hat{\mathbf{y}}$. This improvement term is for gluon contributions only, a similar term must be added if one is interested in quarks as well. Even though hard thermal loops themselves are ultraviolet finite due to their origin from thermal (not quantum) fluctuations [21], the HTL perturbation theory brings with it new UV divergences [22] which must be accounted for with a counter-term $\Delta\mathcal{L}_{HTL}$ which is a function of g and $m^2(1-\delta)$.

The HTL improvement term defines a self energy tensor for gluons, and when resummed to the propagator, corrects the bare propagator into an

effective HTL propagator as follows [23]:

$$\Pi^{\mu\nu}(p) = m^2 \left[\mathcal{T}^{\mu\nu}(p,-p) - n^\mu n^\nu \right] \tag{2.22}$$

$$\mathcal{T}^{\mu\nu}(p,-p) = \left\langle y^\mu y^\nu \frac{p\cdot n}{p\cdot y} \right\rangle_y \tag{2.23}$$

with the tensor $\mathcal{T}^{\mu\nu}(p,-p)$ defined for momenta satisfying $p+q=0$. The self energy tensor can then be separated into transverse and longitudinal parts

$$\Pi^{\mu\nu}(p) = -\Pi_T(p)\left(g^{\mu\nu} - \frac{p^\mu p^\nu}{p^2} - \frac{n_p^\mu n_p^\nu}{n_p^2}\right) - \Pi_L(p)\frac{n_p^\mu n_p^\nu}{(n_p^2)^2}, \tag{2.24}$$

$$\Pi_T(p) = \frac{1}{d-1}(\delta^{ij} - \hat{p}^i\hat{p}^j)\Pi^{ij}(p), \tag{2.25}$$

$$\Pi_L(p) = -\Pi^{00}(p). \tag{2.26}$$

$n^\mu = (1,0)$ represents the rest frame of the heath bath appearing from the breaking of $d+1$ dimensional symmetry to d dimensional rotational symmetry [5], and the vector n_p^μ is defined as $n_p^\mu = n^\mu - \frac{n\cdot p}{p^2}p^\mu$. With these definitions the effective HTL gluon propagator in a general covariant gauge has the form

$$\begin{aligned}\Delta^{\mu\nu}(p) = &-\frac{1}{p^2 - \Pi_T(p)}\left(g^{\mu\nu} - \frac{p^\mu p^\nu}{p^2} - \frac{n_p^\mu n_p^\nu}{n_p^2}\right) \\ &+ \frac{1}{-n_p^2 p^2 + \Pi_L(p)} n_p^\mu n_p^\nu - \rho\frac{p^\mu p^\nu}{(p^2)^2}.\end{aligned} \tag{2.27}$$

The vertex functions and the quark sector are left out of the discussion, but they can be worked out in the same manner from the improvement term in the Lagrangian, which for quarks must be extended to include a term with the spinor fields. To describe imaginary time quantities one must make the necessary conversions discussed previously, e.g. using the discrete Matsubara frequencies, changing the metric to Euclidean and paying attention to the temporal components as they were defined with a $-i$ factor.

Using the HTL framework offers valuable insight to the quark matter equation of state by capturing the problems of infrared sensitive areas into a subtle implementation of perturbation theory and providing more accurate

information about lower order contributions that are subject to said sensitivities. Even though everything was presented in non-zero temperature, hard thermal loops offer a valid effective theory also in the zero temperature limit, where the hard momentum scales correspond to the chemical potential μ instead of T. In contrast to the dimensionally reduced approach, the Matsubara zero-modes ($\omega_n = 0$) are not singled out in the gauge fields to treat the infrared issues. All in all HTL effective theory and DR are very different but together they complement the naive loop expansion rather well, and lay a good groundwork to study the properties of quark matter in low temperatures and high densities.

3 State-of-the-art pressure of quark matter

This chapter is dedicated to the review of state-of-the-art results for the cold and cool quark matter pressure through the evaluation of the equations of state implementing the tools provided in the previous chapter. The primary objective is to introduce results for zero and low but finite temperatures in the limit of all quark masses being zero. Also, the case of non-zero strange quark mass is briefly discussed in the $T = 0$ sector. To demonstrate the value of this highly theoretical investigation, the usage of quark matter EoSs is presented in relation to astrophysical applications concerning properties of neutron stars.

3.1 Pressure at zero temperature

This section consists of the $T = 0$ equation of state first for massless quarks to $\mathcal{O}(g^4)$, with an addition of one NNNLO (next-to-next-to-next-to-leading order) term afterwards, and lastly visiting the work around non-zero strange quark mass.

3.1.1 Leading order, NLO and NNLO contributions to cold quark matter pressure

The cornerstone of the $T = 0$ EoS can be traced back to the result obtained by Freedman and McLerran in their article [24] back in 1977. They applied their work on the thermodynamic potential of relativistic electron gas to strongly interacting matter of massless quarks up to and including $\mathcal{O}(g^4)$

contributions. The connection between electron gas and quark matter serves as a curiosity and a good starting point for the $T = 0$ EoS. At leading order, transferring from electrons to quarks is fairly trivial since the corrections differ only by summing over chemical potentials for all quark flavours, the coupling constant and counting the colors as

$$\begin{aligned} \Omega^{\mathrm{el}}(e^0) &= -\frac{1}{3\pi^2}\frac{1}{4}\mu_{\mathrm{el}}^4 \;\; \rightarrow \\ \Omega^{\mathrm{q}}(g^0) &= -\frac{1}{3\pi^2}\frac{1}{4}\sum_f \mu_f^4 N_c \end{aligned} \tag{3.1}$$

and (with e^2 replaced with $g^2\mathrm{Tr}[\tau^\alpha\tau_\alpha]$, where τ^α are the $\mathrm{SU}(N_c)$ generators)

$$\begin{aligned} \Omega^{\mathrm{el}}(e^2) &= \frac{1}{3\pi^2}\frac{1}{4}\mu_{\mathrm{el}}^4\frac{\alpha}{\pi}\frac{3}{2} \;\; \rightarrow \\ \Omega^{\mathrm{q}}(g^2) &= \frac{1}{\pi^2}\frac{1}{4}\sum_f \mu_f^4\frac{\alpha_s}{\pi}(N_c^2-1), \end{aligned} \tag{3.2}$$

with $\alpha = e^2/4\pi$ and $\alpha_s = g^2/4\pi$.

Proceeding to higher orders in perturbation theory lacks the simplicity of the leading order terms and in [24] some of the more complicated coefficients required numerical evaluation. However, the full $\mathcal{O}(g^4)$ result was calculated analytically in [10], with comparisons to results for finite temperatures, which is the main part of this section.

To begin with, the evaluation of the EoS is performed using modified minimal subtraction scheme ($\overline{\mathrm{MS}}$) and the scale parameter is introduced by defining

$$\int_p \equiv \int \frac{d^dp}{(2\pi)^d} = \Lambda^{-2\epsilon}\left(\frac{e^\gamma\bar{\Lambda}^2}{4\pi}\right)^\epsilon \int \frac{d^dp}{(2\pi)^d}, \tag{3.3}$$

where $\bar{\Lambda}$ is the $\overline{\mathrm{MS}}$ scale, Λ the MS scale, γ the Euler-Mascheroni constant and ϵ is the usual dimensional regularization parameter. Also the following shorthand for the chemical potential sum is used:

$$\sum_f \mu^2 \equiv \boldsymbol{\mu}^2. \tag{3.4}$$

The finite temperature QGP pressure will not be discussed in great detail here as it falls out of the area of interest of this section, but the conver-

gence of low-temperature results will be shown as a difference of the finite temperature and the $T = 0$ results. In the limit of large T/μ, where μ is some configuration of chemical potentials (e.g. equal for all flavours), the pressure is obtained through dimensional reduction as was shown in the previous chapter by splitting the pressure as in eq. (2.19), and evaluating it using the full and effective theories respectively.

In the case of zero temperature, the calculation needs to be divided into IR safe and IR divergent parts. The former corresponds to the free ($\mathcal{O}(g^0)$) potential of eq. (3.1) and a sum of two- and three-loop fermionic graphs (giving also (3.2) at $\mathcal{O}(g^2)$)

$$p_1 \equiv -\Omega_{free} + (I_a + I_b + I_c + I_d + I_f + I_g + I_h)|_{T=0}. \tag{3.5}$$

The I's are related to the diagrams given in Fig. 1 of [10]. The calculations are fully presented in appendices A-D in [10] and only a summary is given below.

Complicated multi-loop diagrams can be simplified by expressing them as combinations of known scalar integrals. This method is explained thoroughly in [25] where it is used for two- and three-loop gluonic vacuum diagrams (with $\mu_f = 0$) by shifts of integration momenta and dividing complicated integrands into several pieces to express them in terms of "basic" scalar integrals with known solutions. The procedure works for fermionic diagrams as well, but one must be careful with the momentum shifts as the temporal fermionic momenta already contain the chemical potential shift. The I loop integrals of (3.5) are presented as products of master integrals (see A.1-A.6 of [10]). The simplest of these are the bosonic and fermionic one-loop integrals $\mathcal{I}^n_m$ and $\tilde{\mathcal{I}}^n_m$, which are defined as

$$\mathcal{I}^n_m \equiv \oint\!\!\!\!\!\!\sum_P \frac{(p_0)^n}{(P^2)^m} \tag{3.6}$$

$$\tilde{\mathcal{I}}^n_m \equiv \oint\!\!\!\!\!\!\sum_{\{P\}} \frac{(p_0)^n}{(P^2)^m}. \tag{3.7}$$

Working in zero temperature the sum-integrals transform into contour integrals over the temporal components as was pointed out in chapter two. The first diagram I_a is in fact rather straightforward as it is a combination of the two integrals above

$$I_a = -(1-\epsilon)(N_c^2-1)\sum_f \left[\tilde{\mathcal{I}}_1^0\left(\tilde{\mathcal{I}}_1^0 - 2\mathcal{I}_1^0\right)\right], \tag{3.8}$$

and yields in $T = 0$ the term (3.2) corresponding to g^2.

From here onwards the diagrams and sum-integrals become increasingly complex and their evaluation here is not of great importance. Generally, one proceeds to separate the diverging part of the integrals and perform the rest straight up in three dimensions while the ultraviolet behaviour needs to be treated with dimensional regularization. The complete result for p_1 comes as follows:

$$\begin{aligned} p_1 = \frac{1}{4\pi^2}\sum_f \mu_f^4 \Bigg[&\frac{N_c}{3} - d_A\left(\frac{g(\bar{\Lambda})}{4\pi}\right)^2 - d_A\Bigg(\frac{2N_f}{3\epsilon} + \frac{2}{3}(11N_c + 4N_f)\ln\frac{\bar{\Lambda}}{\mu_f} \\ &+ \frac{17}{4}\frac{1}{N_c} + \frac{1}{36}(415 - 264\ln 2)N_c + \frac{2}{3}(5 - 4\ln 2)N_f\Bigg)\left(\frac{g(\bar{\Lambda})}{4\pi}\right)^4\Bigg]. \end{aligned} \tag{3.9}$$

Here $d_A = N_c^2 - 1$ and the scale dependency of the running coupling through the renormalization group equation has been presented explicitly. The IR divergent contributions originate from ring diagrams with an overall gluonic loop momentum dressed with insertions of multiple fermion loops (shown in Fig. 1e of [10]). A trick to simplify the ring diagrams is to divide the fermion loop in the gluon self energy diagram to a vacuum ($T = \mu_f = 0$) part and a matter part (the vacuum part subtracted from the original loop). Summing over all the IR divergent parts produces finite terms and at $\mathcal{O}(g^4)$ they present themselves from two cases: a gluon loop with one insertion of vacuum and one of matter self energies, and a summation of all ring diagrams with at least three insertions of the matter self energy part. These diagrams are illustrated in Figure 4 of [10].

The loop diagram corresponding to one vacuum and fermionic matter insertion dubbed, I'_e, can be computed using a convenient form of the fermionic part of the self energy tensor in Feynman gauge

$$(\Pi^f_{\mu\nu})^{ab}(P) = -2g^2 T_F \delta^{ab}\Bigg(2\tilde{\mathcal{I}}^0_1\delta_{\mu\nu} + (P_\mu P_\nu - P^2\delta_{\mu\nu}) \sum\!\!\!\!\!\!\int_{\{P\}} \frac{1}{Q^2(P+Q)^2} - \sum\!\!\!\!\!\!\int_{\{Q\}} \frac{(2Q-P)_\mu (2Q-P)_\nu}{Q^2(Q-P)^2}, \tag{3.10}$$

where $T_F = N_f/2$. From here one can extract the vacuum term by taking T and μ_f to zero and the matter part by subtraction.

After this the computation "dials down" to solving one integral in the $T = 0$ limit for which, similar treatment as in the case of finite temperature can be used. This yields the second part of the pressure:

$$p_2 = \frac{d_A N_f}{4\pi} \sum_f \mu_f^4 \left[\frac{2}{3\epsilon} + 4\ln\frac{\bar{\Lambda}}{\mu_f} + \frac{52}{9} - 4\ln 2\right]\left(\frac{g(\bar{\Lambda})}{4\pi}\right)^4. \tag{3.11}$$

The evaluation of the diagrams with multiple matter insertions, known as the plasmon sum, is more complicated and rather enduring. The computation starts from dividing the vacuum subtracted polarization tensor to two parts with corresponding orthonormal projection operators, and through several auxiliary functions, integral formulas, residues and new variables one is able to present the whole plasmon sum. To spare the reader (and the writer), only the final result and a few explanations are given below.

The plasmon sum gives the following contribution:

$$p_3 = -\frac{d_A}{4\pi^2}(\boldsymbol{\mu}^2)^2\left(\frac{g(\bar{\Lambda})}{4\pi}\right)^4\left[4\ln\left(\frac{g(\bar{\Lambda})}{4\pi}\right)^2 - \frac{22}{3} + \frac{16}{3}\ln 2(1-\ln 2) + \delta + \frac{2\pi^2}{3} + \frac{16}{3}\ln 2\sum_f \frac{\mu_f^4}{(\boldsymbol{\mu}^2)^2} + \frac{F(\boldsymbol{\mu})}{(\boldsymbol{\mu}^2)^2}\right], \tag{3.12}$$

where a new function $F(\boldsymbol{\mu})$ is defined as

$$F(\boldsymbol{\mu}) = -2\boldsymbol{\mu}^2\sum_f \mu_f^2 \ln\frac{\mu_f^2}{\boldsymbol{\mu}^2} + \frac{2}{3}\sum_{f>g}\Bigg[(\mu_f-\mu_g)^2\ln\frac{|\mu_f^2-\mu_g^2|}{\mu_f\mu_g} + 4\mu_f\mu_g(\mu_f^2+\mu_g^2)\ln\frac{(\mu_f+\mu_g)^2}{\mu_f\mu_g} - (\mu_f^4-\mu_g^4)\ln\frac{\mu_f}{\mu_g}\Bigg]. \tag{3.13}$$

As can be seen, the function $F(\boldsymbol{\mu})$ depends on two different flavour sums f and g of the chemical potentials which may seem peculiar at first. This is an artefact of one part of the computation where logarithms that contain flavour sums are expanded in terms of the coupling to $\mathcal{O}(g^4)$ and integrated over to produce terms that couple separate flavour sums together. After this, when performing a leftover contour integration one must consider two different ratios $\mu_f^2/\mu_g^2 > 1$ and $\mu_f^2/\mu_g^2 < 1$ which result in closing the contour differently, and produce the above function [24]. The lone δ in the p_3 result contains a complicated integral that has proven to be very difficult to evaluate in closed form [10] but has a numerical value of approximately -0.8563832. Physically the most interesting thing in the plasmon sum is that there is a term corresponding to $g^4 \ln g^2$ which is absent in p_1 and p_2. Per the discussion in the previous chapter, this term originates from the resummation of individually IR divergent graphs that was needed to obtain a finite result for the pressure, which could not have been done in the naive loop expansion alone.

When combined together, the three parts produce the complete $\mathcal{O}(g^4)$ result for cold and dense quark matter with massless quarks. It can be observed clearly that the UV divergences appearing as $1/\epsilon$ in p_1 and p_2 cancel as is expected for a physical observable.

In figure 3.1 below, results for QGP pressure obtained with dimensional reduction are plotted alongside the above cold quark matter pressure. The figure was plotted for two massless quarks and three colors with the renormalization scale defined as $\bar{\Lambda} = 2\pi\sqrt{T^2 + \mu^2/2\pi^2}$, and the critical temperature with respect to the $\overline{\text{MS}}$ renormalization point $\Lambda_{\overline{\text{MS}}}$ is defined for two quark flavours as $T_c/\Lambda_{\overline{\text{MS}}} = 0.487 \pm 0.023$, with the error sourcing from the definition of $\Lambda_{\overline{\text{MS}}}$ and the extrapolation from measurements made in [26]. It is evident that the difference of low-temperature lines approaches the one of zero-temperature ($P - P_{\text{F-McL}} \to 0$) suggesting that the results describe

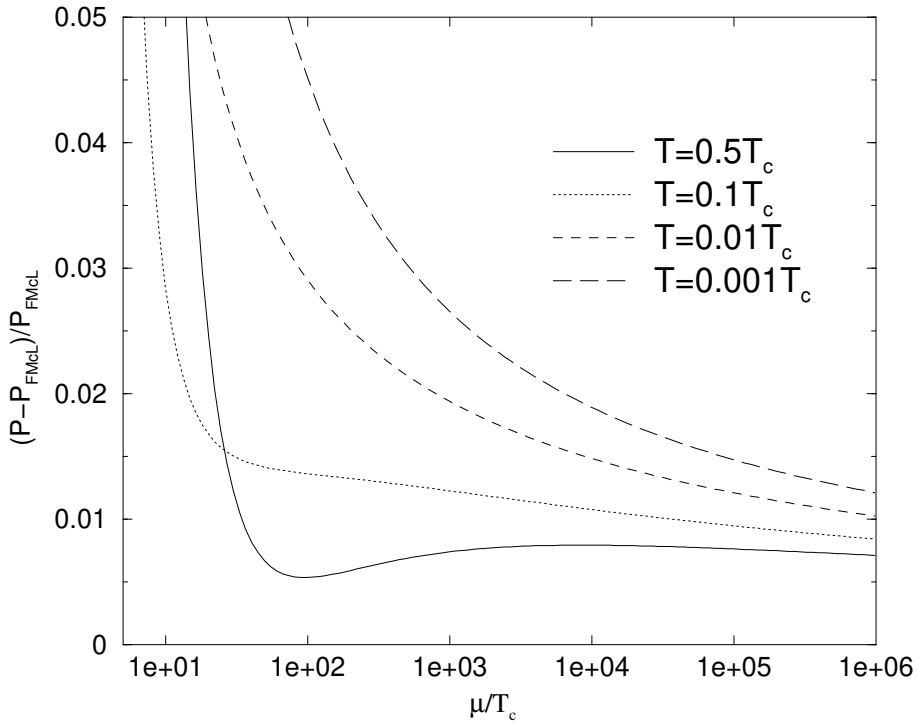

Figure 3.1: The difference of finite and zero-temperature pressures (F-McL for $T = 0$) as a function of the chemical potential configuration μ normalized with the critical deconfinement temperature T_c [10].

well the deconfined phase at higher chemical potential, but as the author pointed out, one should be careful when assessing applicability, due to the fact that dimensional reduction is not very reliable in low temperatures, as can be seen from the gap at lower temperatures from logarithmic divergences, and that the results were analysed only with one configuration of chemical potentials. Nevertheless, the main point of this section was to study the zero-temperature pressure and for that matter the subtleties of the effective theory are not of great concern. Still the comparison has proved somewhat enlightening and serves a purpose to underlay the subject of cool quark matter pressure, a topic to be discussed later.

3.1.2 Leading logarithm in NNNLO pressure at T=0

For a long time equations (3.9), (3.12) and (3.13) contained the only perturbative orders describing cold quark matter pressure. This changed recently after the coefficient for the leading logarithmic contribution of order $g^6\ln^2 g^2$ was calculated in [8] using the methodology of HTL-resummation. The coefficient was calculated in a similar $T = 0$ setting of massless quarks with the exception of simplifying the procedure by assuming the individual chemical potentials to be equal ($\mu_u = \mu_d = \mu_s = \mu_B/3$) with the subscript B referring to baryon chemical potential, which is a sufficient approximation for massless quarks. To study other chemical potential configurations the result can be generalized to include flavour sums without much effort. The pressure for three colors and flavours up to and including $\mathcal{O}(g^6)$ contributions can be presented with numerical coefficients as a sum of the result from the previous subsection and NNNLO terms as

$$p \simeq \frac{3(\mu_B/3)^4}{4\pi^2}\Bigg[1 - 0.636620\alpha_s - 0.303964\alpha_s^2 \ln\alpha_s - \Bigg(0.874355 + 0.911891 \ln\frac{\bar{\Lambda}}{\mu_B/3}\Bigg)\alpha_s^2\Bigg] + c_{3,2}\alpha_s^3 \ln^2\alpha_s + c_{3,1}\alpha_s^3 \ln\alpha_s + c_{3,0}\alpha_s^3, \qquad (3.14)$$

where instead of $g^2/4\pi$, α_s was used. The last three terms contain the new coefficients $c_{3,i}$, and the new coefficient that was computed in [8] is $c_{3,2}$. Pictorially the HTL-resummed loops can be represented as in figure 3.2 below. The double gluonic lines imply the resummed propagators and vertices; remembering the discussion in chapter two, ghost vertices do not require resummation as the (semi-)soft momenta occupy only the gluonic lines. Also, one should note the absence of fermion loop diagrams, which follows from the fact that (at least at $T = 0$) fermionic lines contribute to the analytic expansion in α_s.

As was shown previously, the logarithmic contributions arise in the soft IR sensitive regions, which is also the case with the new higher order terms. In fact, logarithms containing α_s appear when a diagram has integrals where

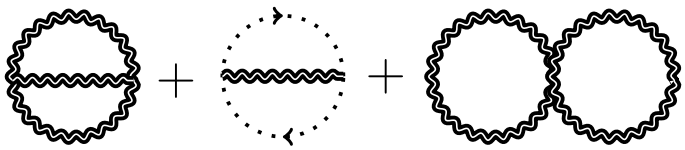

Figure 3.2: Two-loop HTL contribution to the $T = 0$ equation of state [8]. In the first two diagrams the momenta are assigned to the propagators as $P + Q$, P and Q, while in the last there are only P and Q.

the loop momentum is said to be semisoft. The semisoft scale is defined at zero temperature to be $\alpha_s^{1/2}\mu_B \ll P \ll \mu_B$, which brings with it a useful tool. Being much smaller than the hard scale μ_B it allows the use of HTL resummed diagrams, but also being larger than the soft scale $\alpha_s^{1/2}\mu_B$ one can use an expansion of self-energy insertions that appear in the said resummed diagrams. Another simplification for finding the desired logarithm comes from power counting. Introducing a new loop with soft momentum to the diagram (already containing one α_s) brings a contribution of order α_s, meaning that when the term that one is after contributes with $\alpha_s^3 \ln^2 \alpha$, one needs only to consider a case of two separate momenta. Using the argument made about the semisoft scale, the resummed IR sensitive part of the pressure can be cut to four pieces corresponding to the different regions of the momenta. When both momenta are in the hard region, the pressure can be computed from loop expansion; when both are in the soft region, only the HTL-resummed diagrams need to be treated; and in between lies the mixed region, where one momentum is soft and the other is hard, where both need to be treated in either the loop expansion or the HTL approach. This way, the pressure can be defined for two momenta P and Q with the corresponding semisoft scales $\Lambda^{P,Q}$ as

$$
\begin{aligned}
p^{\mathrm{res}}_{\mathrm{IR},\,2} = {} & p^{\mathrm{loop,P;\ loop,Q}}_{\mathrm{IR},\,2}(\{\Lambda^P,\infty\},\{\Lambda^Q,\infty\}) \\
& + p^{\mathrm{res,P;\ loop,Q}}_{\mathrm{IR},\,2}(\{0,\Lambda^P\},\{\Lambda^Q,\infty\}) \\
& + p^{\mathrm{loop,P;\ res,Q}}_{\mathrm{IR},\,2}(\{\Lambda^P,\infty\},\{0,\Lambda^Q\}) \\
& + p^{\mathrm{res,P;\ res,Q}}_{\mathrm{IR},\,2}(\{0,\Lambda^P\},\{0,\Lambda^Q\}). \qquad (3.15)
\end{aligned}
$$

In [8] the leading NNNLO logarithm was calculated from the final part where one can fully apply the HTL resummation.

To proceed with the computation, the diagrams can be worked out in the usual way, with the exception of using HTL-propagators (given in (2.27)) and -vertices. The next step is to reduce the expressions into scalar integrals by working out the Lorentz contractions, which for HTL-propagators and -vertex-functions includes working with the HTL-correction tensors for three and four gluons (in analogy of (2.23)) using Ward identities generalized for the HTL effective theory [27]. After the reduction to scalar sum-integrals (and in zero temperature the sums are taken to continuum), one may employ an expansion of the self-energy insertions due to the semisoft scales of the loops to obtain a series in the asymptotic HTL-mass parameter m_∞^2. The asymptotic mass is related to the effective Debye screening mass given in (2.18) by $m_\infty^2 = m_{eff}^2/2$ (in three spatial dimensions, generally $2 \to d-1$), and it originates from the transverse gluon dispersion relation $\omega^2 = k^2 + \Pi_T(\omega^2, k^2)$, when the polarization tensor is evaluated in the limit of hard momentum [28].

The term corresponding to the leading logarithmic contribution is of $\mathcal{O}(m_\infty^4)$. Using separate cutoffs $\alpha_s^{1/2}\mu_B \ll \Lambda_1^{Q,P} \ll \Lambda_2^{Q,P} \ll \mu_B$ for the two loop-integrals and expanding the integrand around $P/Q = 0$ and $Q/P = 0$ separately, the double logarithm surfaces when the constant terms of the expansions are averaged and $\Lambda_i^{Q,P}$ are given in terms of the soft and hard scales respectively. The full computational details are presented in [27] (for

finite temperatures) and in the appendix of [8]. The coefficient for the $\alpha_s^3 \ln^2 \alpha_s$ term turns out to be

$$c_{3,2} = -\frac{11}{48}\frac{N_c d_a}{(2\pi)^3}\left(\frac{\mu_B^2 N_f}{9\pi}\right)^2, \tag{3.16}$$

where the latter part in brackets comes from m_∞^4, and for three-color three-flavour case takes a numerical value of

$$c_{3,2} = \frac{3(\mu_B/3)^4}{4\pi^2}[-0.266075], \tag{3.17}$$

using the leading order free pressure as a coefficient as in equation (3.14).

Looking at figure 3.3, where the above result is compared with the previous NLO and NNLO $T = 0$ results using renormalization scale $\bar{\Lambda} = 2\mu_B/3$ and a $\overline{\text{MS}}$ renormalization point $\Lambda_{\overline{\text{MS}}} = 0.378$ from the definition of the running coupling α_s [2], it is evident that the partial NNNLO result does not differ greatly from the NNLO pressure. This convergence suggests that the error of the previous perturbative results is indeed small and thus, as will be inspected later, the use of the perturbation theory EoS becomes more valid in the area of study focusing on neutron stars, as the smallness of the error in the EoS reduces its uncertainties and thus increases the accuracy of matching cold quark matter and neutron star matter EoSs [15].

3.1.3 A brief discussion of non-zero strange quark mass in the cold quark matter EoS

All the previous results were obtained in the limit of all quark masses being zero, for $N_f = 3$. The deconfinement energy, i.e. the energy density required to start the confinement-deconfinement phase transition, is around 1 GeV, and for three quark flavours in a cold and dense system it is distributed equally among u, d and s quark chemical potentials, giving the prospect of strange quark production and chemical equilibrium through weak interaction processes since the strange quark mass falls below the third of the total

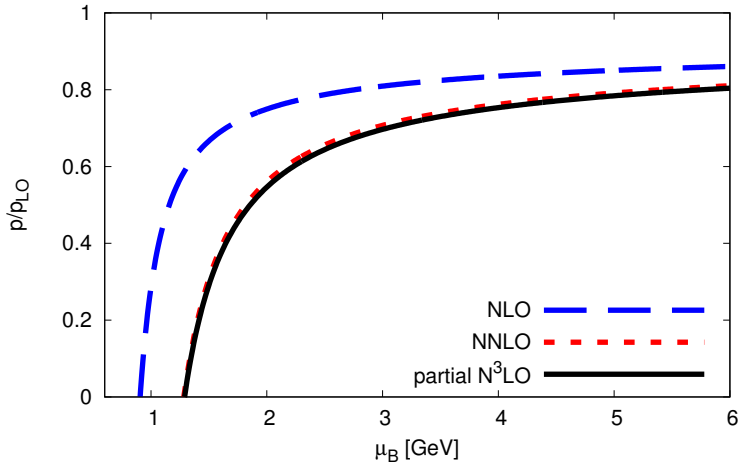

Figure 3.3: A comparison of NLO, NNLO and the double logarithm term in the NNNLO pressures, normalized to the leading order free pressure. [8]

chemical potential assigned to it [4]. From this follows that it is sensible to study cold quark matter also in a setting of one massive and two massless (the u and d quark masses are negligible with respect to m_s) quarks. To strengthen the claim, it has been shown that even at one-loop order in the weak coupling expansion the addition of a non-zero strange quark mass decreases the grand potential by approximately 15% for a fixed mass of 0.1 GeV and a further 8% when using a running mass parameter from the renormalization group equations [29]. This estimation was done for $\mu = 0.6$ GeV and for one massive quark flavour, so the setup does not correspond to cold quark matter, but illustrates the importance of adding a massive quark. The sizeable contribution from non-zero m_s is not limited only to better accuracy in the EoS, but also sets a possibility of stable strange quark ground state. This prospect was studied in [2], but no conclusive evidence could be provided for or against.

Computationally, the strange quark mass brings its own complexities too. To start with, the determination of the grand potential has to be modified to include the new mass parameter, but luckily one does not have

to perform the whole calculation from the beginning. Up to order α_s^2 the grand potential can be split into eight parts $\Omega = \Omega^{m=0} + \Omega^m + \Omega^x_{\mathrm{VM}} + \Omega_{\mathrm{ring}}$ [2]. Here the first term corresponds to a sum of a single quark loop, two- and three-loop two-gluon irreducible vacuum diagrams and a gluon loop with one insertion of vacuum polarization diagram and one insertion of vacuum subtracted matter polarization diagram with zero quark masses and the zero-mass limit of the polarization tensor. The second term is identical, but has to be calculated with a non-zero strange quark mass. The third part corresponds to the previous vacuum-matter gluon loop, but containing a matter polarization tensor in the massless limit and a cross term of massive and massless vacuum quark loop; this part exists only to make a division of the full Ω_{VM} to massless and massive parts. Finally, the last bit is the ring sum, also defined previously, of a gluon loop with at least two matter polarization diagram insertions, to be computed with a massive quark. The reason for this separation is that the massless part can be taken directly from the previous results of section 3.1.1, leaving the remaining terms to be computed.

Another detail that must be taken into account, is the determination of thermodynamic quantities such as pressure and quark number densities. It should be noted that even though one can extract the pressure from the grand potential as $P = -\Omega/V$, when considering physical systems such as compact stars the full structure of the EoS requires stricter thermodynamic consistency set by the conditions of chemical equilibrium and local charge neutrality. These physical conditions imply that the equation $nd\mu = VdP$ does not hold because the full number density n contains higher order terms of α_s, appearing from derivatives e.g. $\partial/\partial\mu(\alpha_s^2)$, than the pressure when it is defined through the equation above. This is not just a massive quark issue as it emerges in the massless case too, but the constraints that arise from charge neutrality and chemical equilibrium for one massive quark, make the

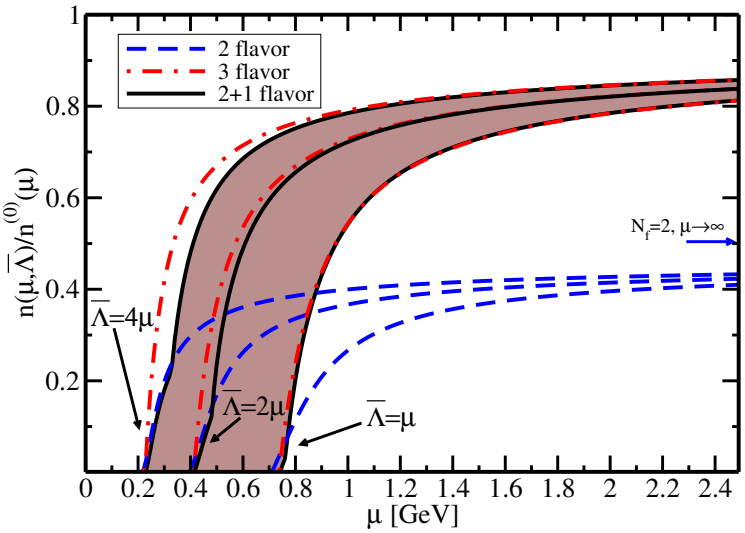

Figure 3.4: Full quark number density at $\mathcal{O}(\alpha_s^2)$ as a function of chemical potential normalised to the free three-flavour number density, for different scenarios of one massive and two or three massless quarks. The uncertainty band originates from varying the $\overline{\text{MS}}$ renormalization scale between μ and 4μ. [2]

determination of the number density and hence the pressure, as it is defined by integration from the number density, even more complicated. Nevertheless, inspecting the EoS without dwelling on the computational details any further reveals a smooth convergence between full number densities for one massive and two massless and the cases two and three massless quarks, as shown in figure 3.4.

What is evident in the figure is that at higher chemical potentials the strange quark mass becomes more and more irrelevant as the uncertainty band overlaps for the one of three massless quarks. Also, in the lower chemical potential region one sees an overlap with the massless two-flavour quark case signalling the lack of energy to produce strange quarks altogether. What should be noted about chemical potential below 1 GeV is that it corresponds to the area of the confined phase where weak coupling expansions

loses its predictive power and also does not describe the phase structure of deconfinement accurately.

3.2 Pressure at low but finite temperatures

An attempt to replicate the previous calculations to include non-vanishing temperatures provides a greater challenge as one has to consider thermal sum-integrals without the simplifying zero-temperature limit. In an earlier work [30], deconfined QCD matter pressure was evaluated at arbitrary μ and T in a weak coupling expansion by performing the necessary resummations using full theory self energies without any effective theory simplifications. This produced quite heavy calculations and numerical results after a lot of work, but also resulted in smooth interpolation between different limits for μ ant T acquired from effective theories. A somewhat more effortless method to study the finite-temperature sector relies on the notion that only soft contributions to the pressure require resummation. This was presented later in [20] and its results are collected in this section.

The starting point for the evaluation lies on a seemingly trivial relation that despite of its outlook simplifies the task considerably. To separate the soft contributions one can add and subtract from the full resummed (res) QCD pressure $p^{\text{res}}_{\text{QCD}}$ the soft part, and end up with a difference $p^{\text{res}}_{\text{QCD}} - p^{\text{res}}_{\text{soft}}$ which contains inherently only hard contributions. The appearance of only hard momenta means that both of these terms can be evaluated directly in the naive loop expansion, leaving the full pressure in the following form:

$$p^{\text{res}}_{\text{QCD}} = p^{\text{naive}}_{\text{QCD}} - p^{\text{naive}}_{\text{soft}} + p^{\text{res}}_{\text{soft}}. \tag{3.18}$$

Furthermore, as one is always inclined to do as little work as possible, the soft sector can be split up between the static (Matsubara zero-mode) and non-static sectors. This division brings out the two effective theories that were discussed in the previous chapter; the static sector is treated in dimensional

reduction while the non-static sector with momenta k being of order m_{eff} is handled in the HTL-framework. This yields the pressure in the simple form of

$$p_{\mathrm{QCD}} = p_{\mathrm{QCD}}^{\mathrm{naive}} + p_{\mathrm{DR}}^{\mathrm{res}} - p_{\mathrm{DR}}^{\mathrm{naive}} + p_{\mathrm{HTL}}^{\mathrm{res}} - p_{\mathrm{HTL}}^{\mathrm{naive}}, \tag{3.19}$$

where the two differences labelled as $p_{\mathrm{DR}}^{\mathrm{corr.}}$ and $p_{\mathrm{HTL}}^{\mathrm{corr.}}$ (implying the corrections to DR and HTL pressures) are UV finite and can be evaluated using previously attained results and techniques.

The naive loop expansion pressure and the resummed dimensional reduction term can be acquired straight away from [10] similarly as the $T = 0$ result was, but now the matching coefficients are evaluated in finite temperature. The naive pressure up to $\mathcal{O}(\alpha_s^4)$ reads

$$p_{\mathrm{QCD}}^{\mathrm{naive}}(T,\mu)/T = T^3\left[\alpha_{\mathrm{E1}} + g^2\alpha_{\mathrm{E2}} + \frac{g^4}{(4\pi)^2}\alpha_{\mathrm{E3}}\right], \tag{3.20}$$

with the first two matching coefficients being (α_{E3} is left to be read from eq. (3.16) of [10] as it is rather space consuming)

$$\alpha_{\mathrm{E1}} = \frac{\pi^2}{45N_f}\sum_f\left[d_A + \left(\frac{7}{4} + 30\bar{\mu}^2 + 60\bar{\mu}^4\right)d_F\right] \tag{3.21}$$

$$\alpha_{\mathrm{E2}} = -\frac{d_A}{144N_f}\sum_f\left[C_A + \frac{T_F}{2}(1+12\bar{\mu}^2)(5+12\bar{\mu}^2)\right]. \tag{3.22}$$

Here a new dimensionless variable $\bar{\mu} \equiv \mu/(2\pi T)$ was utilised, and a new group theoretic factor d_F is defined by $d_F \equiv \delta_{ii} = N_c N_f$.

The UV finiteness of the function $p_{\mathrm{DR}}^{\mathrm{corr.}}$ implies the cancellation of $1/\epsilon$ poles of the two terms it contains. As it happens, the naive DR pressure vanishes in dimensional regularization, with the exception of the UV and IR poles, because it only contains integrals with no scales. With the cancellation of the UV poles, the only pole in the pressure is an IR pole, which is also regulated by $1/\epsilon$ (and is equal to the UV poles with an opposite sign). This leaves the resummed DR term to represent the DR pressure correction by

itself. The DR pressure correction then reads

$$p_{\mathrm{DR}}^{\mathrm{corr.}}/T = p_{\mathrm{DR}}^{\mathrm{res}}/T = \frac{d_A}{12\pi} m_{eff}^3 + \frac{d_A C_A}{(4\pi)^2} g_{\mathrm{E}}^2 m_{eff}^2 \left[-\frac{1}{4\epsilon} - \frac{1}{3} - \ln \frac{\bar{\Lambda}}{2m_{eff}} \right] + \frac{d_A C_A^2}{(4\pi)^3} g_{\mathrm{E}}^4 m_{eff} \left[-\frac{89}{24} - \frac{\pi^2}{6} + \frac{11}{6} \ln 2 \right]. \tag{3.23}$$

The effective mass is the one introduced earlier and the effective coupling comes from the aforementioned EQCD with the form $g_{\mathrm{E}}^2 = g^2 T + \mathcal{O}(g^4)$.

The term $p_{\mathrm{HTL}}^{\mathrm{res}}$ is obtainable from a ring diagram dressed with self energy insertions as before, but now the resummation is performed in the HTL framework outlined earlier, implying the use of specific HTL self energy tensors. This results in a sum-integral over the non-static Matsubara modes containing logarithms of the self energy that need to be evaluated directly, rather than expanding the logarithms as can be done when evaluating the naive HTL counterpart. Only the result will be presented below, as the calculation of $p_{\mathrm{HTL}}^{\mathrm{corr.}}$ will be carried out in detail in chapter four. The HTL pressure sums up to be

$$p_{\mathrm{HTL}}^{\mathrm{corr.}} = \frac{d_A m_{eff}^4}{256\pi^2} f_{\mathrm{HTL}}(T/m_{eff}). \tag{3.24}$$

The function $f_{\mathrm{HTL}}(T/m_{eff})$ has well defined limits for $T \to 0$ and $T \to \infty$ that can be applied in the appropriate cases.

When studying the full p_{QCD} result in the limits of high and low temperatures, a couple things stand out. First, in the high temperature limit $T \gg m_{eff}$, the f_{HTL} function behaves as $\mathcal{O}(m_{eff}^2/T^2)$ and dies out very rapidly with respect to the naive and DR pressures, and the pressure produces a known high temperature limit of [10]. Second, the low temperature limit $T \to 0$ converges smoothly to the previous $T = 0$ result as the DR pressure approaches zero faster and the corresponding limit of f_{HTL} contains a logarithm of T that together with the coefficient $(m_{eff}^2)^2$ cancels similar logarithmic terms from the zero-temperature limit of the α_{E3} matching

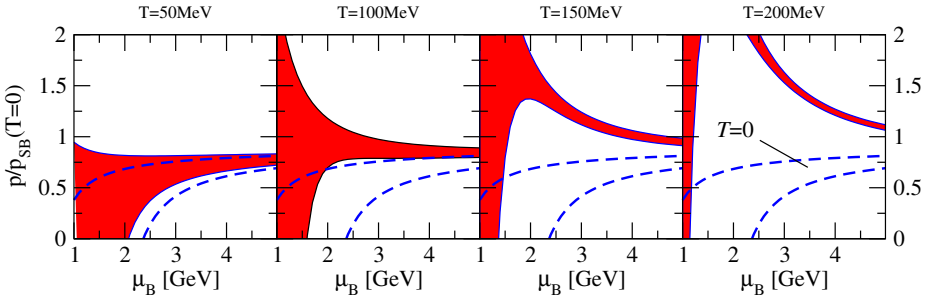

Figure 3.5: Pressure of cool quark matter as a function of baryon chemical potential, with the uncertainty band produced by variation of $\bar{\Lambda}$. The previous zero-temperature result is illustrated as the dashed blue line. [20]

coefficient. This behaviour serves as a good pointer that the combined effective theory approach is sufficient to describe the low-temperature and high density quark matter equation of state.

In Fig. 3.5 we present the cool quark matter EoS at different temperatures ranging from 50 to 200 MeV as a function of baryon chemical potential normalized to the $T = 0$ free pressure (SB indicating the Stefan-Boltzmann pressure which is taken at $T \to 0$ limit). The difficulty of choosing the renormalization scale was resolved in [20] by using a root mean square of the scales corresponding to the zero-temperature and zero chemical potential scales, giving $\bar{\Lambda} = \sqrt{(0.723 \times 4\pi T)^2 + (2\mu_B/3)^2}$, with a two-loop running coupling $\alpha_s(\bar{\Lambda})$ and the QCD renormalization point $\Lambda_{\mathrm{QCD}} = 378$ MeV. It is evident from the graph that smaller temperatures start overlapping with the $T = 0$ result, as is the range of applicability of the weak coupling expansion seen as the blow-up of the uncertainty band when advancing towards the deconfinement chemical potential near $\mu_B = 1$ GeV.

3.3 The role of the quark matter EoS in neutron stars

Before continuing to the HTL calculation of the next chapter, it is useful to take a quick look at the uses of the previously presented EoS results in real applications. To find systems with as high densities as assumed in the above computations one needs to look no further than space. While other compact systems such as stable strange quark stars that can be described with quark matter EoS may exist, the only direct astrophysical data to compare the EoS with corresponds presumably to neutron stars (could also be quark stars), obtained most recently from gravitational waves emitted by a binary neutron star (BNS) inspiral, detected by the LIGO-Virgo collaboration in 2017 [31]. The first indirect detection of gravitational waves from a BNS system dates back to 1982, when the energy loss of a BNS orbit was observed suggesting GW emission [32].

As stated previously, the perturbative QCD EoS can be applied only at high densities (at zero or low temperature), meaning that the earlier results cannot be applied directly to describe the full neutron star EoS. The other end of the density scale is also well determined by an effective theory called chiral effective theory (CET). CET is a low energy effective theory for very low densities where the degrees of freedom are pions and nucleons, in a setting where the chiral symmetry is spontaneously broken, yielding the framework of chiral perturbation theory with an expansion parameter m_π/p_F, where m_π is the pion mass and p_F the Fermi momentum [33]. The CET approach has been successfully used to achieve NNNLO results of low density nuclear matter energy [34]. Between the two extremes of nuclear and quark matter lies the elusive region of neutron star matter. The reason one is interested in the two boundaries is that using the known results for the two EoSs, one can interpolate between them to constrain the realistic

neutron star EoS by matching.

The neutron star matter EoS is typically approximated by a polytropic relation between pressure and number density, using small density intervals, assuming that [15]

$$p_i(n) = \kappa_i n^{\gamma_i}, \tag{3.25}$$

where κ_i are constants, n is the baryon density (number of baryons per volume) and γ_i are polytropic indices. The subscript i denotes dividing the EoS into intervals in the baryon chemical potential $\mu_i < \mu_B < \mu_{i+1}$, with the requirement that pressure and energy density are continuous when the intervals are matched. Uniformly varying the parameters γ_i and μ_i produce an ensemble of EoSs depending on the choice of the constraints and limits employed.

One way to utilise the gravitational wave data is by calculating constraints for neutron stars through a dimensionless constant called tidal deformability λ. In the inspiral phase of a BNS system, both stars experience the effect of tidal forces where they exert a quadrupolar tidal field $\mathcal{E}_{ij}$ to the other, which in turn induces a quadrupole moment $\mathcal{Q}_{ij}$ on the star. Tidal deformability is defined as a constant between these two tidal effects as [35]

$$\mathcal{E}_{ij} = -\lambda \mathcal{Q}_{ij}. \tag{3.26}$$

The coefficient λ on the other hand, is related to the radii of the stars via [15]

$$\lambda_i = \frac{2}{3} k_2^{(i)} \left[\frac{c^2}{G} \frac{R_i}{M_i} \right]^5, \tag{3.27}$$

where $k_2^{(i)}$ is a constant called Love number (of the second kind) and R_i and M_i are the radii and masses of the stars (G is of course the gravitational constant and c the speed of light). The original analysis of the LIGO-Virgo data reports an upper bound for λ to be 800 with 90% confidence, which serves as an upper bound for the mass-radius curves and conveniently drops EoSs that would support stars that go over the boundary. This limit was

later dropped to 580 with the same confidence [36], but this section follows the analysis with the looser constraint of 800.

Neutron star masses vary typically from one to two solar masses ($M_\odot$) [37]. The mass distribution data gives another constraint for the EoS ensemble, namely the maximum mass limit of neutron stars. A good estimate from an earlier study for the lower limit for $M_{\max}$ comes from observations of a binary system of a radio pulsar NS with a mass of $1.90 - 2.18 M_\odot$ (with 99.73% confidence) [38] and a white dwarf, giving a boundary of $M_{\max} > 2M_\odot$ [15]. Later analyses of the recent LIGO-Virgo GW data, combined with data from gamma ray bursts of the same merger and the lower limit from the radio pulsar observations, produced an estimate of $2.01^{+0.04}_{-0.04} < M_{\mathrm{TOV}}/M_\odot < 2.16^{+0.17}_{-0.15}$. M_{TOV} is the Tolman-Oppenheimer-Volkoff limit for non-rotating cold NSs related to the maximum mass of uniformly rotating NSs by $M_{\max} = 1.20^{+0.02}_{-0.05} M_{\mathrm{TOV}}$ [39]. Using these mass limits helps to remove EoSs that cannot support stars with high enough masses from the ensemble.

With these observational constraints cutting out unphysical EoSs, the matching process (outlined in [15] and [40]) can be performed with increased accuracy. Starting from the low density EoS from CET up to a number density of $n = 1.1 n_0$ where n_0 denotes the nuclear saturation density, one can use either a soft or stiff EoS (the NNNLO result from [34]), meaning a lower or an upper limit of the pressure at that fixed number density. This EoS is known with ±24% accuracy, which suggests using a cold quark matter EoS with the same uncertainty as an end point. This is achieved when the baryon chemical potential is around 2.6 GeV, and the polytropic pressure is then interpolated between these limits. From the point of view of this thesis, the most interesting part of the matching process is the end point of the interpolation. The studies mentioned above used the EoS from [2], where the strange quark mass was also taken into account, in the form of

a fitting function depending on chemical potential and the renormalization scale with numerical coefficients. The renormalization scale is implemented as a dimensionless parameter defined as $X = 3\bar{\Lambda}/\mu_B$ and it is varied in a scale of [1,4]. This shows the power of employing a high density quark matter limit, since one can discard all EoSs that cannot be matched to any value of X at $\mu_B = 2.6$ GeV. After all the possible EoSs are interpolated, a final physical constraint is used; all the EoSs in the ensemble must satisfy $c_s^2 < 1$ as the speed of sound cannot exceed the speed of light, i.e. all superluminal EoSs can be kicked out of the family.

The results of this process are depicted in Figure 3.6 as a plot of pressure with respect to energy density using quadrutropic and tritropic (smaller picture) pressure. Here, the tidal deformability and mass constraints are implemented in the color coding as follows: the cyan region corresponds to EoSs that cannot support stars over $2M_\odot$, the green region is for tidal deformabilities (calculated with $M = 1.4M_\odot$) $\lambda < 400$, the violet region for $400 < \lambda < 800$ and the red region for $\lambda > 800$. The red region can be excluded with 90% credence as was stated before. The black dashed lines enforce the further mass limit of $M_{\max} < 2.16M_\odot$. The blue and orange areas correspond to the CET and cold quark matter EoSs respectively. Now that the EoSs are under control, the astrophysical quantities of interest, namely the mass-radius curves of neutron stars, can be obtained from TOV equations in general relativity [2]

$$\begin{aligned} dM(r) &= 4\pi r^2 \epsilon(r) dr, \\ dP(r) &= -\frac{G(P(r) + \epsilon(r)(M(r) + 4\pi r^3 P(r))}{r(r - 2GM(r))}. \end{aligned} \tag{3.28}$$

For neutron stars one can use the allowed EoS ensemble determined above which is inserted through energy density $\epsilon(r)$, and the pressure is determined by choosing a central value P at the centre of the star and integrating from $r = 0$ to the surface where the pressure tends to zero. The mass-radius clouds

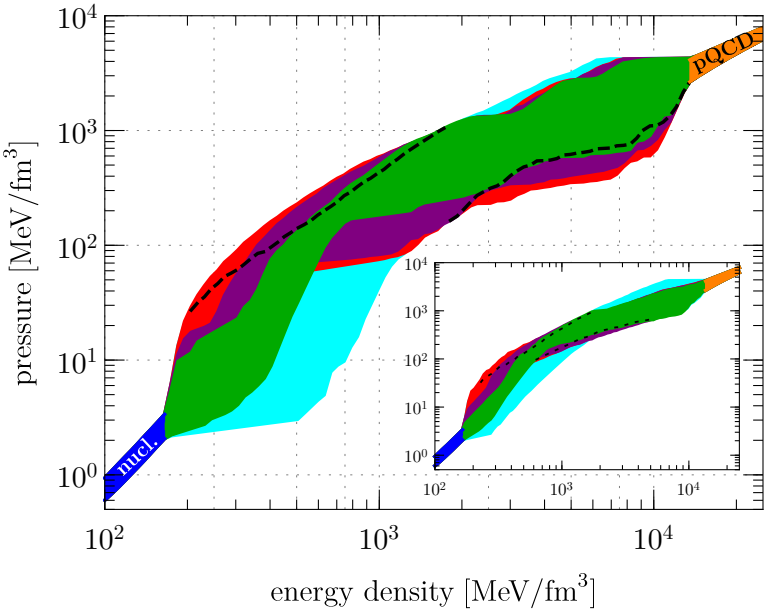

Figure 3.6: Quadru- and tritropic pressure ensembles with respect to energy density. Explanations are offered in the main text. [15]

for the polytropic EoS ensemble can be found in Fig. 1 of [15].

4 First non-analytic terms at low T: HTL ring sum

Non-analytic contributions, in terms of the coupling constant, start appearing in the pressure when the resummation of infrared contributions is taken into account. A glimpse of this was seen in the zero-temperature plasmon sum of section 3.1 which produced a logarithmic contribution of $g^4 \ln(g)$. At low temperatures, the first non-analytic terms can be extracted from the effective HTL treatment of the non-static Matsubara modes, following the procedure of section 3.2. The leading order non-analytic contribution can be expressed as an HTL ring sum, where the correction to the gluon propagator is derived from the HTL improvement term in the Lagrangian, given in section 2.5. Taking only the non-static terms and simplifying the calculation a bit by subtracting the pressure of a free massless boson $\Omega_0 = \oint\!\!\!\!\!\!-_K \log[K^2]$ as a counter-term, the starting point of the calculation is the following [20]

$$\begin{aligned} p^{\mathrm{res}}_{\mathrm{HTL}} = &-\frac{(d-1)d_A}{2} \oint\!\!\!\!\!\!-_K{}' \log\left[1+\frac{\Pi_T}{K^2}\right] \\ &-\frac{d_A}{2} \oint\!\!\!\!\!\!-_K{}' \log\left[1+\frac{\Pi_L}{K^2}\right]. \end{aligned} \tag{4.1}$$

The transverse and longitudinal self energy functions follow from the corrected inverse propagator after the HTL self energy has been separated into the corresponding parts by imposing rotational symmetry and Ward identity [22]. The functions are defined in three spatial dimensions by

$$\frac{\Pi_T}{K^2} = \frac{1}{2}\frac{m^2}{\omega_n^2+k^2} - \frac{m^2}{2k^2}\left(1-\frac{i\omega_n}{2k}\log\left[\frac{i\omega_n+k}{i\omega_n-k}\right]\right) \tag{4.2}$$

$$\frac{\Pi_L}{K^2} = \frac{m^2}{k^2}\left(1-\frac{i\omega_n}{2k}\log\left[\frac{i\omega_n+k}{i\omega_n-k}\right]\right), \tag{4.3}$$

where m is the asymptotic HTL mass related to the effective mass m_{eff}. The primes introduced in the sum-integrals imply that the zero-mode is left out, which enables one to write them as

$$\begin{aligned}
\sum\!\!\!\!\!\!\int_K{}' \log\left[1+\frac{\Pi_T}{K^2}\right] &= \sum\!\!\!\!\!\!\int_K \log\left[1+\frac{\Pi_T}{K^2}\right] - T\int_{\mathbf{k}} \log\left[1+\frac{\Pi_T(\omega_n=0)}{K^2}\right] \\
&= \sum\!\!\!\!\!\!\int_K \log\left[1+\frac{\Pi_T}{K^2}\right] - 0, \\
\sum\!\!\!\!\!\!\int_K{}' \log\left[1+\frac{\Pi_L}{K^2}\right] &= \sum\!\!\!\!\!\!\int_K \log\left[1+\frac{\Pi_L}{K^2}\right] - T\int_{\mathbf{k}} \log\left[1+\frac{\Pi_L(\omega_n=0)}{K^2}\right] \\
&= \sum\!\!\!\!\!\!\int_K \log\left[1+\frac{\Pi_L}{K^2}\right] - T\int_{\mathbf{k}} \log\left[1+\frac{m^2}{k^2}\right].
\end{aligned}$$

Starting from the transverse term, the sum-integral can be transformed into a contour integral with the help of the Bose distribution function $n_B(\omega_n) = (e^{i\beta\omega_n}-1)^{-1}$, and taking ω to the real axis by a change of variables $\omega_n \to -i\omega$. This yields,

$$\sum\!\!\!\!\!\!\int_K \log\left[1+\frac{\Pi_T}{K^2}\right] = \frac{1}{2\pi i}\int_{\mathbf{k}} \oint_C d\omega \log\left[1+\frac{\Pi_T(-i\omega)}{K^2}\right] n_B(-i\omega). \tag{4.4}$$

The contour C encloses the poles $\omega_n = 2\pi nT$ of n_B on the imaginary axis. The logarithm has branch cuts following from the quasiparticle dispersion relation $-\omega^2 + k^2 + \Pi_T(\omega) = 0$ when $\omega = \pm\omega_T$, due to $\omega_T^2 - k^2 = \Pi_T(\omega_T)$, with the self energy taking the role of quasiparticle mass, and at $w = \pm k$ which are related to Landau damping, which means that when spacelike gauge fields propagate in the plasma they lose energy when scattering with hard particles. At this point, the subtraction of Ω_0 pays off because the logarithm approaches zero when ω is taken to infinity. This is convenient because now the contour that wraps the poles of n_B can be deformed to enclose the branch cuts on the real axis ranging from $\omega_T \to -k \to k \to \omega_T$, instead of three separate regions from $-\omega_T \to -\infty$, $-k \to k$ and $\omega_T \to \infty$. As a result the contour consists of eight pieces (integrating clockwise):

$$\oint_C \to \int_{-\omega_T+i\epsilon}^{-k+i\epsilon} + \int_{-k+i\epsilon}^{k+i\epsilon} + \int_{k+i\epsilon}^{\omega_T+i\epsilon} + \int_{\gamma_1} + \int_{\omega_T-i\epsilon}^{k-i\epsilon} + \int_{k-i\epsilon}^{-k-i\epsilon} + \int_{-k-i\epsilon}^{-\omega_T-i\epsilon} + \int_{\gamma_2}.$$

The γ contours represent integrating a half circle with a radius of ϵ which both tend to zero when the limit $\epsilon \to 0$ is taken; by the ML inequality, which states that $|\int_\gamma f(z)dz| \leq Ml(\gamma)$ where l is the arc length of γ and $M = \max|f(z)|_{z\epsilon\gamma}$, the upper limit of the contour integral behaves as ϵ times contributions from the integrand. The quasiparticle and Landau damping parts can be studied separately, but first a few notions about the integrand. The function inside the logarithm is now

$$f(\omega) = 1 + \frac{\Pi_T(-i\omega)}{K^2} = 1 - \frac{1}{2}\frac{m^2}{\omega^2 - k^2} - \frac{m^2}{2k^2}\left(1 - \frac{\omega}{2k}\log\left[\frac{\omega + k}{\omega - k}\right]\right).$$

This function is symmetric in $\omega \to -\omega$ as the latter part with the logarithm transforms as

$$-\frac{(-\omega)}{2k}\log\left[\frac{-\omega + k}{-\omega - k}\right] = -\frac{\omega}{2k}\log\left[\frac{-1}{-1}\frac{\omega - k}{\omega + k}\right]^{-1} = -\frac{\omega}{2k}\log\left[\frac{\omega + k}{\omega - k}\right].$$

In the quasiparticle region ($\omega_T > |\omega| > k$) $f(\omega)$ is negative and thus the logarithm has a discontinuity which allows it to be forced to the principal branch ($-\pi < arg(f(\omega)) \leq \pi$) with the imaginary part approaching $\pm i\pi$ when the limit $\pm i\epsilon \to 0$ is taken. In the Landau damping part, on the other hand, where $|\omega| < k$ and

$$f(\omega) = 1 + \frac{1}{2}\frac{m^2}{k^2 - \omega^2} - \frac{m^2}{2k^2}\left(1 - \frac{\omega}{2k}\log\left[\frac{\omega + k}{\omega - k}\right]\right),$$

such a luxury is out of the question. Another useful identity should also be pointed out:

$$n_B(-\omega) = \frac{1}{e^{-\beta\omega} - 1} = \frac{e^{\beta\omega}}{1 - e^{\beta\omega}} = \frac{e^{\beta\omega} - 1 + 1}{1 - e^{\beta\omega}} = -1 - n_B(\omega).$$

With these definitions in mind, one is well equipped to tackle the quasiparticle contour, which when added up gives:

$$\int_{-\omega_T + i\epsilon}^{-k + i\epsilon} \log[f(\omega)]n_B(\omega) + \int_{k + i\epsilon}^{\omega_T + i\epsilon} \log[f(\omega)]n_B(\omega)$$
$$+ \int_{\omega_T - i\epsilon}^{k - i\epsilon} \log[f(\omega)]n_B(\omega) + \int_{-k - i\epsilon}^{-\omega_T - i\epsilon} \log[f(\omega)]n_B(\omega).$$

Then, taking ω to the negative real axis in the first and last terms and swapping the limits in first and third gives

$$\int_{k-i\epsilon}^{\omega_T-i\epsilon} \log[f(\omega)](-1-n_B(\omega)) + \int_{k+i\epsilon}^{\omega_T+i\epsilon} \log[f(\omega)]n_B(\omega)$$
$$- \int_{k-i\epsilon}^{\omega_T-i\epsilon} \log[f(\omega)]n_B(\omega) - \int_{k+i\epsilon}^{\omega_T+i\epsilon} \log[f(\omega)](-1-n_B(\omega)),$$

after which the terms with $\pm i\epsilon$ can be combined and ϵ taken to zero to produce:

$$\begin{aligned}
&- \int_{k-i\epsilon}^{\omega_T-i\epsilon} \log[f(\omega)](1+2n_B(\omega)) + \int_{k+i\epsilon}^{\omega_T+i\epsilon} \log[f(\omega)](1+2n_B(\omega)) \\
&= - \int_k^{\omega_T} [(\log|f(\omega)| - i\pi) + (\log|f(\omega)| + i\pi)](1+2n_B(\omega)) \\
&= 2\pi i \int_k^{\omega_T} d\omega(1+2n_B(\omega)) = 4\pi i \left[T \log \frac{1-e^{-\beta\omega_T}}{1-e^{-\beta k}} + \frac{1}{2}(\omega_T - k) \right]. \qquad (4.5)
\end{aligned}$$

For the Landau damping contribution, one has the two terms:

$$\begin{aligned}
&\int_{-k+i\epsilon}^{k+i\epsilon} \log[f(\omega)]n_B(\omega) + \int_{k-i\epsilon}^{-k-i\epsilon} \log[f(\omega)]n_B(\omega) \\
&= \int_{-k+i\epsilon}^{k+i\epsilon} \log[f(\omega)]n_B(\omega) - \int_{-k+i\epsilon}^{k+i\epsilon} \log[f(\omega)](-1-n_B(\omega)) \\
&= \int_{-k+i\epsilon}^{k+i\epsilon} \log[f(\omega)](1+2n_B(\omega)) \\
&= \int_{-k+i\epsilon}^{0} \log[f(\omega)](1+2n_B(\omega)) + \int_0^{k+i\epsilon} \log[f(\omega)](1+2n_B(\omega)) \\
&= \int_0^{k-i\epsilon} \log[f(\omega)](1-2(1+n_B(\omega))) + \int_0^{k+i\epsilon} \log[f(\omega)](1+2n_B(\omega)) \\
&= - \int_0^k (\mathfrak{Re}\log[f(\omega)] - i\mathfrak{Im}\log[f(\omega)])\,(1+2n_B(\omega)) \\
&+ \int_0^k (\mathfrak{Re}\log[f(\omega)] + i\mathfrak{Im}\log[f(\omega)])\,(1+2n_B(\omega)).
\end{aligned}$$

With the cancellation of the real parts of the logarithm, the result can be written into a more compact form:

$$-2i \int_0^k d\omega\phi_T(1+2n_B(\omega)), \qquad (4.6)$$

with the angle $\phi_T = -\mathfrak{Im}\log[f(\omega)]$.

Combining the two results (4.5) and (4.6) the contour integral defined in (4.4) takes the form:

$$\begin{aligned}\sum\!\!\!\!\!\!\int_K \log\left[1+\frac{\Pi_T}{K^2}\right] &= \frac{1}{2\pi i}\int_{\mathbf{k}}\oint_C d\omega \log\left[1+\frac{\Pi_T(-i\omega)}{K^2}\right] n_B(-i\omega) \\ &= 2\int_{\mathbf{k}}\left[T\log\frac{1-e^{-\beta\omega_T}}{1-e^{-\beta k}}+\frac{1}{2}(\omega_T-k)\right]-\frac{1}{\pi}\int_{\mathbf{k}}\int_0^k d\omega\phi_T(1+2n_B(\omega)). \quad (4.7)\end{aligned}$$

The procedure for the longitudinal part is similar, with the exception of the zero-mode subtraction term, and yields:

$$\begin{aligned}\sum\!\!\!\!\!\!\int_K \log\left[1+\frac{\Pi_L}{K^2}\right] =& 2\int_{\mathbf{k}}\left[T\log\frac{1-e^{-\beta\omega_L}}{1-e^{-\beta k}}+\frac{1}{2}(\omega_L-k)-\frac{T}{2}\log(1+\frac{m^2}{k^2})\right] \\ &-\frac{1}{\pi}\int_{\mathbf{k}}\int_0^k d\omega\phi_L(1+2n_B(\omega)), \quad (4.8)\end{aligned}$$

with ϕ_L defined the same way as its transverse counterpart.

Having obtained the resummed HTL pressure, the next step is to make the integrals ultraviolet finite. As was explained in the previous chapter, this can be achieved by subtracting the naive HTL pressure to correct order from the resummed result. The naive pressure can be acquired by expanding the grand potential logarithms in terms of the self energy functions as [20]:

$$p_{\mathrm{HTL}}^{\mathrm{naive}} = -d_A \sum\!\!\!\!\!\!\int_K{}' \left[\frac{d-1}{2}\frac{\Pi_T}{K^2}+\frac{1}{2}\frac{\Pi_L}{K^2}-\frac{1}{2}\left(\frac{d-1}{2}\frac{\Pi_T^2}{(K^2)^2}+\frac{1}{2}\frac{\Pi_L^2}{(K^2)^2}\right)\right]+\mathcal{O}(g^6). \quad (4.9)$$

The evaluation of equations (4.7)-(4.9) put together needs to be performed numerically using e.g. Mathematica, which will be left out here as it provides no further physical or calculational insights. The result after numerical evaluation is the one cited earlier, equation (3.24):

$$p_{\mathrm{HTL}}^{\mathrm{corr.}} = p_{\mathrm{HTL}}^{\mathrm{res.}} - p_{\mathrm{HTL}}^{\mathrm{naive}} = \frac{d_A m_{eff}^4}{256\pi^2} f_{\mathrm{HTL}}(T/m).$$

The function f_{HTL} has the following low- and high-temperature limits [20]:

$$f_{\mathrm{HTL}}|_{T\to 0} \to 4\ln\frac{T}{m} + 11 - 4\gamma - \frac{2\pi^2}{3} + \frac{14\ln 2}{3} + \frac{16\ln^2 2}{3} + 4\ln\pi - \delta - \frac{64\pi}{3}\frac{T}{m} - \frac{32\pi^2}{9}\left(\frac{T}{m}\right)^2\left(\ln\frac{T}{m} - \ln\frac{4}{\pi} - \gamma + \frac{\zeta^{'}(2)}{\zeta(2)}\right) + \mathcal{O}((T/m)^{8/3}), \tag{4.10}$$

$$f_{\mathrm{HTL}}|_{T\to\infty} \to -\frac{0.006178(1)}{(T/m)^2} + \mathcal{O}((m/T)^3). \tag{4.11}$$

Here, γ is the Euler-Mascheroni constant, δ is the previously introduced constant from equation 3.12 and ζ is the Riemann zeta function.

From the $T \to 0$ limit, one can see the first non-analytic terms of the pressure. The effective mass squared is proportional to the coupling g^2, so the logarithmic terms in the low temperature limit behave as $g^4 \ln g$ and $g^6 \ln g$, which should not seem peculiar by now since resumming the infrared sensitive sector contributes through logarithmic terms as was established in chapter 3.

5 Conclusions

As must be evident by now, introducing non-zero temperature and density to quantum field theory brings along new intricate concepts and subtleties, and is in no fashion a trivial matter. Two important subjects that have been discussed are effective theories and the integration of classical, quantum and observational physics.

One thing both laypersons and experts have in common is the recognition that quantum field theory is extremely complicated, even without the complications of a thermal medium. Studying observables in thermal perturbation theory in QCD leads to an increasing number of coupled fermionic and bosonic fields with divergences of infrared and ultraviolet nature. While vacuum renormalization solves the ultraviolet behaviour, the accounting of infrared divergences by resummation in the perturbative expansion is cumbersome and enduring. The admirable goal of preserving one's sanity provided the driving force to create effective approaches to simplify the complexities regarding the infrared troubles.

One approach concentrates on the separation of different scales arising from the addition of thermal and finite density effects. The infrared issues relating to the Matsubara zero modes of bosonic fields can in high temperatures be captured by integrating out the fermionic hard scale πT or $\pi\mu$, and studying exclusively the zero-mode contribution. As a result, the imaginary-time argument vanishes from the integrals leaving only spatial dimensions to be dealt with, hence providing an effective theory of dimensional reduction. Dimensional reduction is a well defined theory, even if it relies on the error that appears from series truncation to be small in order to be sustainable.

The effective theory has brought much ease to the analytical evaluation of high-temperature observables in QGP and also provides tools for somewhat lower temperatures in cool quark matter.

What also was observed was that above tree level, when the external bosonic momenta are restricted to a soft scale of gT or $g\mu$ and the loop momentum integration is restricted to the hard scale of T or μ, one-loop diagrams that behave as $g^2T^2/P^2\times$(corresponding tree-lvl amplitude) would produce a tree level result thus breaking the perturbative expansion. This produced the branch of hard-thermal-loop physics which solves infrared issues by a resummation of soft propagators and vertices. The resummation procedure produces additional momentum dependent terms, which when calculated unearth a specific HTL self energy function. When computing the wanted soft observables, the addition of the self energy function shields the perturbation expansion by preserving the correct loop order. HTL resummation can be compiled to an effective Lagrangian containing a so-called HTL improvement term for bosonic (and if needs be also fermionic) fields, but some issues have been found regarding the renormalizability of the theory at higher orders. Overlooking the problem of renormalization, HTL effective theory provides a valuable tool for power counting to simplify complicated situations by singling out problematic areas or separating calculations to different momentum sectors and treating them according to their momentum scale. The strength of HTL effective theory was shown e.g. in section 3.1.2 when the leading NNNLO logarithm was extracted by the separation of soft and semi-soft scales, or in chapter four when the non-analytic contributions of infrared resummation needed to be accounted for.

It is evident that effective theories complement the perturbation series very well. To verify their robustness, one can always check if different limits e.g. of low and high temperature converge to known full theory results, as was the case with dimensional reduction in 3.1.1 or as can be seen from

the cool quark matter result, where previously known limits could be reproduced. It is well known that Nature is indeed a complicated entity to study, and using well crafted tools to simplify gauging its secrets should be encouraged. Approximations and justification by error estimation have always been present in physics and often cannot be escaped when chasing results even with the most rigorous analytical calculations.

The cold QCD pressure is now partly known to next-to-next-to-next-to-leading-order, with the highest known term being of order $g^6 \ln^2 g^2$. The leading NNNLO logarithm term was shown to almost overlap with the NNLO result. It is a useful thing to be able to verify that the higher order corrections do not wander far off from the previous results as this informs that the weak coupling series is on the correct course. However, this also poses the question of how meaningful it is to continue exploring even higher corrections with smaller contributions to the observables. This kind of convergence is of course not always granted, and thanks to effective theories extracting the complicated coefficients has become a bit easier. But still, as one could go on to ever higher order corrections, one should also ask how long is it reasonable to carry on.

The present state of thermal field theory is a good indicator of the progression and integration of physics. Not does it only employ the modern quantum field theory quantized from classical, it also utilises the work of thermodynamics and classical statistical mechanics gathered and tweaked into a form that accommodates the needs of quantum mechanics. If putting together two branches of quantum physics with a long history starting form classical theories was not enough, the current observations from a neutron star merger adds general relativity and astrophysics to the mix. The Relativistic Heavy Ion Collider where temperatures around the critical temperature of the deconfined phase were obtained might still be the only direct source into thermal QCD, but the LIGO-Virgo data is a milestone between

highly theoretical and observational physics. The gravitational waves might not have carried direct information about cold or cool quark matter, but as was presented, the value of cold and dense QCD equation of state manifested in constraining the neutron star EoS from above with respect to density. It is reasonable to expect that the relationship of theory and observation in strongly interacting dense matter will only tighten and converge to the point where some day the questions of stable quark matter, whether it will be a strange star or a quark core inside a neutron star, can be studied not only in theory but with data as well. One must stand in awe, of Nature and the achievements of science, when an event that must be so mundane in the universe entwines decades of research in fundamental theories together.

Bibliography

[1] H. Fritzsch, "The history of QCD," *CERN Courier*, October 2012.

[2] A. Kurkela, P. Romatschke, and A. Vuorinen, "Cold Quark Matter," *Phys. Rev. D 81, 105021*, 2010.

[3] D. J. Gross and F. Wilczek, "Asymptotically Free Gauge Theories," *Phys. Rev. D Vol.8(10)*, 1973.

[4] J. I. Kapusta, *Finite-temperature field theory.* Cambridge University Press, 1989.

[5] M. Laine and A. Vuorinen, *Basics of Thermal Field Theory.* Springer, 2018.

[6] W. Greine, S. Schramm, and E. Stein, *Quantum Chromodynamics.* Springer, 2nd ed., 2002.

[7] K. Huang, *Statistical Mechanics.* John Wiley & Sons, 2nd ed., 1987.

[8] T. Gorda, A. Kurkela, P. Romatschke, M. Säppi, and A. Vuorinen, "NNNLO pressure of cold quark matter: leading logarithm," *Phys. Rev. Lett. 121, 202701*, 2018.

[9] A. Motornenko, J. Steinheimer, V. Vovchenko, S. Schramm, and H. Stoecker, "Equation of state for hot QCD and compact stars from a mean field approach," *Phys. Rev. C 101, 034904*, 2020.

[10] A. Vuorinen, "The pressure of QCD at finite temperatures and chemical potentials," *Phys.Rev. D 68, 054017*, 2003.

[11] P. de Forcrand, "Simulating QCD at finite density," *PoS LAT2009, 010*, 2010.

[12] A. Bazavov *et al.*, "Equation of state in (2+1)-flavor qcd," *Phys. Rev. D 90, 094503*, 2014.

[13] D. Boyanovsky, "Phase transitions in the early and the present universe: From the big bang to heavy ion collisions," *arxiv:hep-ph/0102120v2*, 2001.

[14] Illustration by Alan Stonebraker.

[15] E. Annala, T. Gorda, A. Kurkela, and A. vuorinen, "Gravitational-wave constraints on the neutron-star-matter Equation of State," *Phys. Rev. Lett. 120, 172703*, 2018.

[16] J. Fleischer, F. Jegerlehner, O. V. Tarasov, and O. L. Veretin, "Two-loop QCD corrections of the massive fermion propagator," *Nucl.Phys. B539, 671-690*, 1999.

[17] O. Philipsen, "Debye screening in the QCD plasma," *arXiv:hep-ph/0010327v1*, 2000.

[18] S. Nadkarni, "Dimensional reduction in finite-temperature quantum chromodynamics," *Phys. Rev. D 27 (1983)*, 1983.

[19] K. Kajantie, M. Laine, K. Rummukainen, and M. Shaposhnikov, "Generic rules for high temperature dimensional reduction and their application to the standard model," *Nucl.Phys. B 458, 90-136*, 1996.

[20] A. Kurkela and A. Vuorinen, "Cool quark matter," *Phys. Rev. Lett. 117, 042501*, 2016.

[21] E. Braaten and R. D. Pisarski, "Soft amplitudes in hot gauge theories: A general analysis," *Nucl. Phys. B 337*, 1990.

[22] J. O. Andersen, E. Braaten, and M. Strickland, "Hard thermal loop resummation of the thermodynamics of a hot gluon plasma," *Phys. Rev. D 61, 014017*, 2000.

[23] J. O. Andersen, E. Petitgirard, and M. Strickland, "Two-loop HTL Thermodynamics with Quarks," *Phys. Rev. D 70, 045001*, 2004.

[24] B. A. Freedman and L. D. McLerran, "Fermions and gauge vector mesons at finite temperature and density III," *Phys. Rev. D 16 1169*, 1977.

[25] P. Arnold and C. Zhai, "The three loop free energy for pure gauge QCD," *Phys. Rev. D 50, 7603-7623*, 1994.

[26] S. Gupta, "A precise determination of T(c) in QCD from scaling," *Phys. Rev. D 64, 034507*, 2001.

[27] J. O. Andersen, E. Braaten, E. Petitgirard, and M. Strickland, "HTL perturbation theory to two loops," *Phys. Rev. D 66, 085016*, 2002.

[28] P. Levai and U. W. Heinz, "Massive gluons and quarks and the equation of state obtained from SU(3) lattice QCD," *Phys. Rev. C 57, 1879-1890*, 1998.

[29] E. S. Fraga and P. Romatschke, "The role of quark mass in cold and dense perturbative QCD," *Phys. Rev. D 71, 105014*, 2005.

[30] A. Ipp, K. Kajantie, A. Rebhan, and A. Vuorinen, "The pressure of deconfined QCD for all temperatures and quark chemical potentials," *Phys. Re. D 74, 045016*, 2006.

[31] B. P. Abbott *et al.*, "GW170817: Observation of gravitational waves from a binary neutron star inspiral," *Phys. Rev. Lett. 119, 161101*, 2017.

[32] J. H. Taylor and J. M. Weisberg, "A new test of general relativity - Gravitational radiation and the binary pulsar PSR 1913+16," *Astrophys. J. 253, 908-920*, 1982.

[33] W. Weise, "Nuclear chiral dynamics and phases of QCD," *Prog. Part. Nucl. Phys. 67, 299-311*, 2012.

[34] I. Tews, T. Krüger, K. Hebeler, and A. Schwenk, "Neutron matter at next-to-next-to-next-to-leading order in chiral effective field theory," *Phys. Rev. Lett. 110, 032504*, 2013.

[35] E. E. Flanagan and T. Hinderer, "Constraining neutron star tidal Love numbers with gravitational wave detectors," *Phys. Rev. D77, 021502*, 2008.

[36] B. P. Abbott *et al.*, "GW170817: Measurements of neutron star radii and equation of state," *Phys. Rev. Lett. 121, 161101*, 2018.

[37] F. Ozel, D. Psaltis, R. Narayan, and A. S. Villarreal, "On the mass distribution and birth masses of neutron stars," *Astrophys. J. 757, 55*, 2012.

[38] J. Antoniadis *et al.*, "A massive pulsar in a compact relativistic binary," *Science 340, 6131*, 2013.

[39] L. Rezzolla, E. R. Most, and L. R. Weih, "Using gravitational-wave observations and quasi-universal relations to constrain the maximum mass of neutron stars," *Astrophys. J. 852, L25*, 2018.

[40] A. Kurkela, E. S. Fraga, J. Schaffner-Bielich, and A. Vuorinen, "Constraining neutron star matter with quantum chromodynamics," *Astrophys. J. 789, 127*, 2014.